SIMULATION OF CURRENT CROWDING MITIGATION IN GAN CORE-SHELL NANOWIRE LED DESIGNS

A Thesis
Presented to
The Academic Faculty

by

Benjamin James Connors

In Partial Fulfillment
of the Requirements for the Degree
Masters in the
School of Electrical and Computer Engineering

Georgia Institute of Technology
August 2011

SIMULATION OF CURRENT CROWDING MITIGATION IN GAN CORE-SHELL NANOWIRE LED DESIGNS

Approved by:

Dr. Benjamin Klein, Advisor
School of Electrical and Computer Engineering
Georgia Institute of Technology

Dr. D.P. Yoder
School of Electrical and Computer Engineering
Georgia Institute of Technology

Dr. David Citrin
School of Electrical and Computer Engineering
Georgia Institute of Technology

Date Approved: July, 2011

ACKNOWLEDGEMENTS

To my parents, for allowing me to pursue those things I desired, and to my advisor for having the sense to tell me when those desires were out of scope.

TABLE OF CONTENTS

	Page
ACKNOWLEDGEMENTS	iii
LIST OF TABLES	vi
LIST OF FIGURES	vii
LIST OF SYMBOLS AND ABBREVIATIONS	ix
SUMMARY	x
CHAPTER	
1 Introduction	1
2 Gallium Nitride Materials System	2
Gallium Nitride Growth	2
P-type Gallium Nitride	2
N-type Gallium Nitride	3
Internal Electric Fields	3
3 Nanowire Devices	4
Construction	4
P-type Growth	4
P-n Junctions in Nanowires	5
Core-Shell Nanowires	5
4 Current Crowding	7
Current Crowding in Core-Shell Nanowires	7
Current Crowding in Similar Structures	9
Current Crowding and Device Efficiency	12
Simulation of Current Crowding in Core-Shell Nanowires	14

5 Simulated Current Crowding 18
Initial Constant Core Doping 18
Core Doping With Increased Doping in the Shell Contact Region 20
Alpha 0.001 20
Alpha 1 23
Alpha 100 26
Core Doping With Increased Doping in the Core Contact Region 28
Alpha 0.001 28
Alpha 1 31
Alpha 100 33
Extending Doping into the Isolated Core 36
Summary of Results 39
6 Simulated Efficiency 40
High Doping in the Shell Contact Region 41
High Doping in the Core Contact Region 43
Summary of Results 45
7 Conclusions 47
APPENDIX A: Derivation of Junction Voltage Model 46
REFERENCES 50

LIST OF TABLES

	Page
Table 1: Primary Simulation Parameters	17
Table 2: Efficiency Values at Similar Bias Points	44

LIST OF FIGURES

Page

Figure 1: Core-Shell Nanowire Structure used in this work 9

Figure 2: Current Crowding in Core-Shell Nanowire. Current streamlines were calculated using TiberCAD, as described below in this thesis. 10

Figure 3: Model for striped laser used by Thompson[1] 12

Figure 4: Doping profiles generated by generating function 16

Figure 5: Current Distribution in Constant Doped Case 19

Figure 6: Conduction band with direct recombination overlaid in constant doped case 19

Figure 7: Junction voltage as a function of junction axial position z in constant doping case. 20

Figure 8: Doping in Alpha 0.001 with high doping in the shell contact region 21

Figure 9: Current Distribution In Alpha 0.001 high doping in the shell contact region 21

Figure 10: Conduction Band with Direct Recombination overlaid in Alpha 0.001 high doping in the shell contact region 22

Figure 11: Junction voltage in alpha 0.001 with high doping in shell contact region 22

Figure 12: Doping in Alpha 1 with high doping in the shell contact region 23

Figure 13: Current Distribution In Alpha 1 high doping in the shell contact region 24

Figure 14: Conduction band with direct recombination overlaid in Alpha 1 high doping in the shell contact region 24

Figure 15: Junction voltage in alpha 1 with high doping in shell contact region 25

Figure 16: Doping in Alpha 100 with high doping in the shell contact region 26

Figure 17: Current Distribution In Alpha 100 high doping in the shell contact region 26

Figure 18: Conduction band with direct recombination overlaid in Alpha 100 high doping in the shell contact region 27

Figure 19: Junction voltage in alpha 100 with high doping in shell contact region 27

Figure 20: Doping in Alpha 0.001 with high doping in the core contact region 28

Figure 21: Current Distribution In Alpha 0.001 high doping in the core contact region 29

Figure 22: Conduction band with direct recombination overlaid in Alpha 0.001 high doping in the core contact region 29

Figure 23: Junction voltage in alpha 0.001 with high doping in core contact region 30

Figure 24: Doping in Alpha 1 with high doping in the core contact region 31

Figure 25: Current Distribution In Alpha 1 high doping in the core contact region 31

Figure 26: Conduction band with direct recombination overlaid in Alpha 1 high doping in the core contact region 32

Figure 27: Junction voltage in alpha 1 with high doping in core contact region 32

Figure 28: Doping in Alpha 100 with high doping in the core contact region 33

Figure 29: Current Distribution In Alpha 100 high doping in the core contact region 34

Figure 30: Conduction band with direct recombination overlaid in Alpha 100 high doping in the core contact region 34

Figure 31: Junction voltage in alpha 100 with high dopant concentration in core contact region 35

Figure 32: Doping Diagram of Device with profile extended into core region above shell 36

Figure 33: Current Density in alpha 0.001 with doping profile extended into core beyond shell 37

Figure 34: Conduction band with direct recombination overlaid in Alpha 0.001 high doping in the core contact region with doping profile extended beyond shell37

Figure 35: Junction voltage in alpha 0.001 with high doping in core contact region, with the profile extended beyond the shell 38

Figure 36: Calculated Efficiency for all cases with high doping in the shell contact region 43

Figure 37: Calculated Efficiency for all cases with high dopant concentration in core contact region 45

Figure 38: Constant core potential seen in constant doped core-shell nanowire 47

Figure 39: Comparison of modeled and simulated junction voltage 52

Figure 40: Comparison of modeled and simulated junction current density 52

LIST OF SYMBOLS AND ABBREVIATIONS

GaN	Gallium Nitride
Si	Silicon
Mg	Magnesium
LED	Light Emitting Diode
VLS	Vapor Liquid Solid
LEEBI	Low Energy Electron Beam Irradiation

SUMMARY

Core-shell nanowire LEDs are light emitting devices which, due to a high aspect ratio, have low substrate sensitivity, allowing the possibility of low defect density GaN light emitting diodes. Current growth techniques and physical non-idealities make the production of high conductivity p-type GaN for the shell region of these devices difficult. Due to the structure of core-shell nanowires and the difference in conductivity between n-type and p-type GaN, the full junction area of a core-shell nanowire is not used efficiently. To address this problem, a series of possible doping profiles are applied to the core of a simulated device to determine effects on current crowding and overall device efficiency. With a simplified model it is shown that current crowding has a possible dependence on the doping in the core in regions other than those directly in contact with the shell. The device efficiency is found to be improved through the use of non-constant doping profiles in the core region with particularly large efficiency increases related to profiles which modify portions of the core not in contact with the shell.

CHAPTER 1

INTRODUCTION

The application of nanoscale growth and fabrication techniques to light emitting diodes, laser diodes and other optoelectronic devices has increased recently as these techniques improve and become more widely accessible. Amongst nanoscale device structures, nanowires provide not only benefits of reduced feature size, but also decreased substrate sensitivity preventing lattice relaxation[2]. Nanowire growth has matured to a point where gallium nitride nanowires are possible and often the target of experimental research [3-6]. The use of nanowire devices for gallium nitride light emitting devices could provide a fast route to highly efficient gallium nitride nanoscale light emitters without having to wait for advances in materials growth and processing to provide high quality material[7]. However, nanowire structures are affected by issues related to their small diameters; in particular, pinning of the Fermi level at the surface has been shown to affect axial nanowire structures, resulting in current flow issues and surface recombination[8]. In order to reduce adverse effects of the axial nanowire structure, a different structure has been developed consisting of a narrow radius core, with a radial shell region grown around it. This device, the core-shell nanowire, provides a reduction in surface recombination, while simultaneously drastically increasing the junction area [9, 10]. Unfortunately, due to device geometry and gallium nitride material properties, these devices suffer from current crowding [11, 12]. This thesis analyzes the issue of current crowding through simulation, and proposes design solutions to alleviate this problem through changes to the doping profile of core-shell nanowire structures. The data is evaluated in regards to increasing the efficiency and usable light production within the core-shell nanowire structure.

CHAPTER 2

GALLIUM NITRIDE MATERIALS SYSTEM

The state of growth techniques in the gallium nitride materials system and relevant material parameters are important to the simulation of core-shell nanowires. LED devices made in this materials system need to be simulated with the effects of defects and other phenomena taken into account for accurate device modeling.

Gallium Nitride Growth

The growth of gallium nitride is a difficult process due to a lack of suitable substrates, the temperature insensitivity of gallium nitride, and the materials resistance to chemicals[13]. Commercially, gallium nitride substrates are only available from a small number of vendors, and are expensive. Most gallium nitride devices are grown using non-lattice matched substrates. Special techniques must be employed to successfully deposit gallium nitride on these substrates [13-15]. The resulting gallium nitride growth contains a high density of defects. The high defect densities lead to large intrinsic electron concentrations due to several specific defects, such as Ga vacancies and interstitials [7, 16-20].

P-type Gallium Nitride

Acceptor doping in gallium nitride is a process that took several years to accomplish, and is still a difficult procedure. The key difficulty in acceptor doping in gallium nitride is the high defect concentration in gallium nitride leading to acceptor compensation[21, 22]. Due to work by several researchers, appropriate growth

conditions were found to grow GaN with defect densities low enough to allow for successful acceptor doping[21, 23]. However, due to acceptor passivation, most likely in the form of hydrogen, the acceptor doping did not produce GaN materials with high enough concentrations of holes for p-n junction formation. Continued effort eventually lead to p-type GaN produced by acceptor doping followed by one of two possible depassivation techniques. The earliest used method was Low Energy Electron Beam Irradiation (LEEBI)[22]. This technique used an electron beam striking the acceptor doped p-type material, which would depassivate the acceptor dopants. This technique was soon followed by a thermal anneal process which also depassivated acceptors[23]. This does not solve the problem caused by increased defect densities in GaN. The high intrinsic electron population from the increased defect density, compensates any p-type doping up to a certain level in GaN[16]. While the intrinsic donor concentration reduces the effectiveness of acceptor doping, p-n junction formation is still possible. In addition to reduced acceptor doping capabilities, the hole mobility in GaN is very low relative to the electron mobility[21, 22, 24-26]. The high defect density and necessarily increased acceptor species doping only reduces the mobility of holes in GaN further[25].

N-type Gallium Nitride

Donor doping in GaN is almost exclusively done with silicon [27-30]. The production of n-type material with few defects and large electron concentrations is easily attainable when compared to the production of p-type GaN. The activation energy of Si in GaN is between 17 meV and 12 meV[31]. Compensation of donor dopants does occur in GaN, this has been noted to occur through vacated Ga sites[32]. When Silicon takes the place of a Nitrogen site some compensation is possible. However, the compensation of donors in GaN is of little concern as all intrinsic growths of GaN reported have an intrinsic n-type carrier concentration. The effects of high donor dopant

concentrations have been documented to start affecting mobility above Si doping concentrations of $1x10^{18}$ cm^{-3} [33].

Internal Electric Fields

The hexagonal symmetry of the GaN crystal lattice gives rise to spontaneous and strain-induced piezoelectric polarization, which can generate significant internal electric fields. Large differences between the lattice constants of gallium nitride, growth substrates, and common compounds used for quantum wells leads to significant strain and hence piezoelectric electric fields in many III-nitride devices[34]. High internal electric fields can impact device operation in a variety of ways, including the quantum confined Stark effect and associated shifts in optical transitions in quantum well devices[35]. The use of nanowire devices has been proposed as a method of reducing the negative effects of the built-in polarization fields in gallium nitride devices, , as nanowires offer a method of reducing overall strain on the device thereby reducing piezoelectric polarization effects[35].

CHAPTER 3

NANOWIRE DEVICES

Nanowires are a class of semiconductor device which sit at the boundary between quantum mechanics and classical mechanics. These devices have feature sizes from the tens of nanometers to micrometers, with very large aspect ratios. With large nanowire devices, a classical simulation of the drift-diffusion equations can be used to model many of the properties of the structure. All nanowires provide for increased surface areas from the large aspect ratio, and decreased defect densities through substrate insensitivity from narrow diameters.

Construction

Several approaches have been studied for the growth of nanowires. Nanowire fabrication requires a preferential 1 dimensional growth with a single crystal consistency through a number of possible methods. Carbon nanotube confinement of semiconductor growth has been used in early work[36]. A more common method is the unconfined growth of nanowires through vapor liquid solid growth (VLS) [3, 37-39]. In this method a catalyst is used, which at a certain temperature can form a compound in both the liquid and the solid phase with the growth material. When the system is kept at this temperature a preferential one dimensional growth occurs at the interface of the catalyst and the remaining compound. The radius of the structure can be determined by the radius of the catalyst nanodots deposited on the substrate [37, 40]. This growth produces wire-like structures typically of good quality with few defects. Using molecular beam epitaxy it is also possible to grow nanowires through confined growth which relies on vapor liquid solid growth techniques. These methods allow for growth rate and dimensions to be controlled by a predefined matrix. This method has been used by researchers at the

National Institute of Standards and Technology collaborating with our group. The confined VLS method produces structured arrays of nanowires which are straight and of high crystalline quality. Other methods of controlled unconfined growth exist with the use of temperature as the growth controlling parameter [4, 41]. The unconfined speed of growth and eventual length of nanowires can be controlled through reactant gas pulsing techniques[5]. Due to narrow diameters nanowires are very substrate insensitive, allowing for direct growth of GaN nanowires on materials like silicon[42] and sapphire[43].

P-n Junctions in Nanowires

P-type GaN nanowires have similar issues to those of bulk GaN when doped with acceptors. However, due to the smaller size of the nanowire, defect densities in nanowire structures are reduced. This would ideally result in less compensation of acceptor dopants; however, hole mobilities in p-type GaN nanowires are still low, on the order of 10 $cm^2/V*s$[43]. The unintentional n-type doping has been shown to be non-negligible in nanowire p-n junctions, which in early works produced p-n junctions without donor doping the n-type portion of the nanowire[6]. Many early homojunction p-n diodes consist of a p-type nanowire grown on top of an n-type nanowire (axial p-n junctions). These devices often contend with problems common to bulk GaN devices, such as trap levels and poor acceptor doping efficiencies [44, 45]. One particular problem in GaN nanowire homojunctions is that of surface states and surface recombination [46-48].

Core-Shell Nanowires

Core-shell nanowires take advantage of advanced nanowire growth techniques by growing structures in both axial and radial directions. By carefully controlling the growth conditions, preferential growth in either axial or radial directions can be achieved.

Typically this process begins with a VLS technique as described above for the growth of an initial nanowire core [9, 10, 49]. After the nanowire has reached the appropriate length, the growth conditions are changed to achieve radial growth. The preferential radial growth in nanowires can be controlled by careful control of temperature and injection rate of growth species. During this part of the growth, epitaxy occurs in the radial direction of the nanowire. The radial growth can be performed with different dopants and different materials. This allows for the creation of nanowires with large p-n junctions, or the creation of radial heterostructures. The benefits of core-shell nanowire devices stem from the large surface area of the junction and the modified current path, which limits the effects of surface recombination. The alignment of non-polar surfaces along the junction allow for unique properties beneficial to structures containing quantum wells. Core-shell devices provide the possibility of a more efficient nanowire structures for nanoscale light emitting devices[50]. In unconfined device fabrication core-shell nanowires can be grown by exploiting preferential growth speed between axial and radial epitaxy with gallium flow[3] . In confined device fabrication the core and shell deposition processes can be accomplished in a two step process where the speed of growth is controlled through similar growth species flow rates.

CHAPTER 4

CURRENT CROWDING

Current crowding occurs when a large current density is isolated to a relatively small region within a device. This problem is seen in many semiconductor devices for a variety of reasons. In gallium nitride devices this problem often comes from material properties, but also may be due to geometrical factors. Commonly this is seen in GaN mesa LED structures due to the geometry of the device and the difference in conductivity between the n and p-type layers [51, 52]. Another case where current crowding commonly occurs is in strip lasers where the effect is almost purely due to the small contact size in relation to the rest of the device[1]. In this chapter the effects of current crowding in core-shell nanowires will be described and models from previous works which are applicable will be discussed.

Current Crowding in Core-Shell Nanowires

Current crowding in core-shell nanowires is a combined geometric, materials, and contact size issue. The combination of large aspect ratio, reduced conductivity in the p-type material, and small contact size results in a non-uniform current distribution. The geometry of the core-shell nanowire device produces a large junction area relative to the device diameter. This presents a very large surface for current to cross in the device. The path that it takes from the shell contact to the core contact is related to the path of least resistance through the device. With a highly conductive n-type core, the shell conductivity and the shell contact are the important factors for determining current flow through the device[11]. In the initial design considered in this thesis, the shell electrode is small and placed around the circumference of the shell of the device at the farthest point from the core contact, as seen in Fig. 2. This shell contact configuration is chosen

to allow the light generated by the LED to escape the device. When current flow is simulated in this device, the current density crowds at the point on the junction at the same axial height as the shell contact (Fig. 1, Fig. 2). Further, the region of highest current concentration is directly beneath the edge of the shell contact closest to the core contact. When the shell contact is extended to the full height of the shell, the current crowding is reduced; however, the area beneath the edge of the shell contact closest to the core contact of the device still has the highest current density [12, 51].

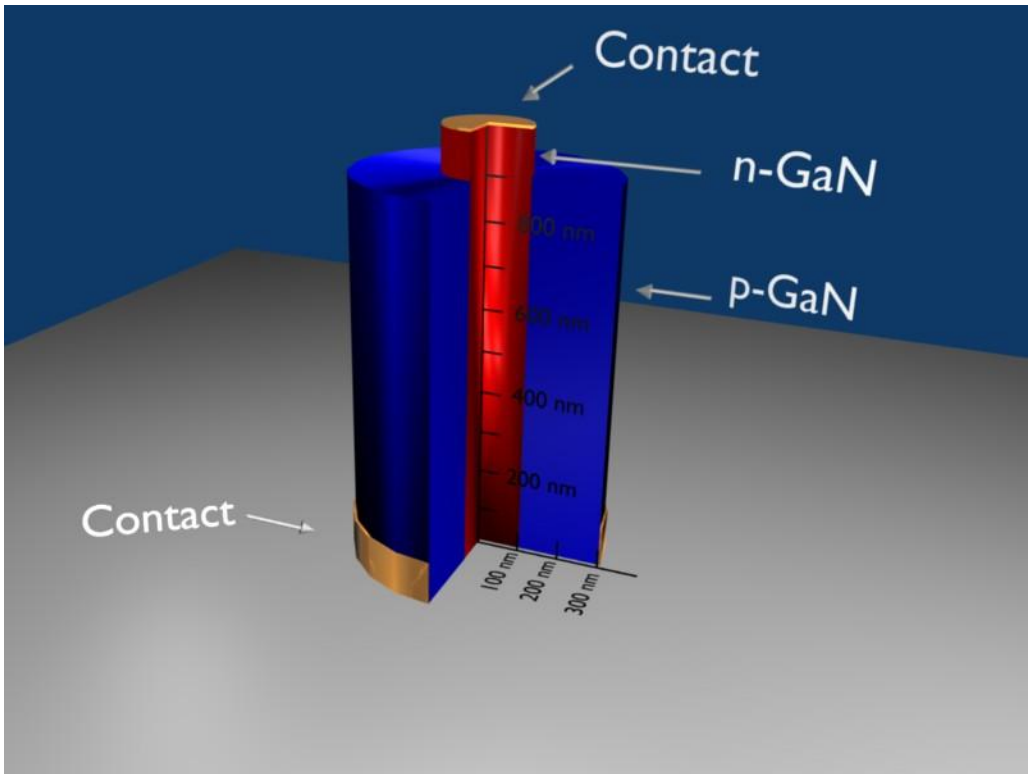

Figure 1: Core-Shell Nanowire Structure used in this work

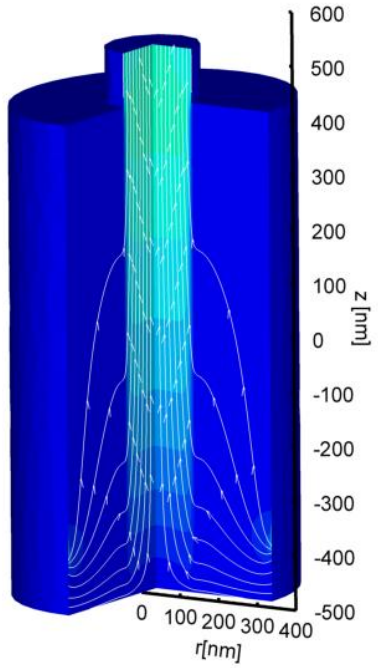

Figure 2: Current Crowding in Core-Shell Nanowire. Current streamlines were calculated using TiberCAD, as described below in this thesis.

Current Crowding Analysis in Similar Structures

The current distribution in bulk GaN LEDs and laser diodes has been investigated previously using simplified models [1, 51, 52]. The models used in these works involve replacing the junction with an idealized diode and using basic electrical network analysis to determine the current and voltage relations within the device. This begins with establishing an equipotential surface. In Thompson's text[1] the n-type region of a p-n junction strip laser was assumed to have an equipotential surface on the n-type side, as it was highly conductive with constant doping. Although, not applicable to the case of non-constant doping profiles, using some of the results in the works by Fletcher, Thompson, Guo et. al., and other researchers [53, 54] a more thorough understanding of the current crowding problem can be developed. The work performed by Thompson is most applicable to the situation presented by a core-shell nanowire. Thompson modeled the current in a strip laser with a narrow contact (Fig. 3) through a simplification of the

voltage gradient along the length of the device, relating it to the current crossing a junction using the ideal diode equation. This structure is very similar to the core-shell nanowire structure in that it has a poorly conductive shell on top of a highly conductive region, in addition to having a contact of limited area on the poorly conductive shell. At its core Thompson's analysis is similar to earlier work done by Fletcher on current distribution along an emitter-base junctions in BJTs[54]. A description of Fletcher's work and its application to this work is available in Appendix A. In the work done by Thompson, the current flow through a structure with a contact of reduced area and a poorly conducting region used equation 1 (originally developed by Fletcher) to describe the relation between the voltage in the shell region (upper portion of figure 3) to the current crossing the junction into the n-type region of much higher conductivity.

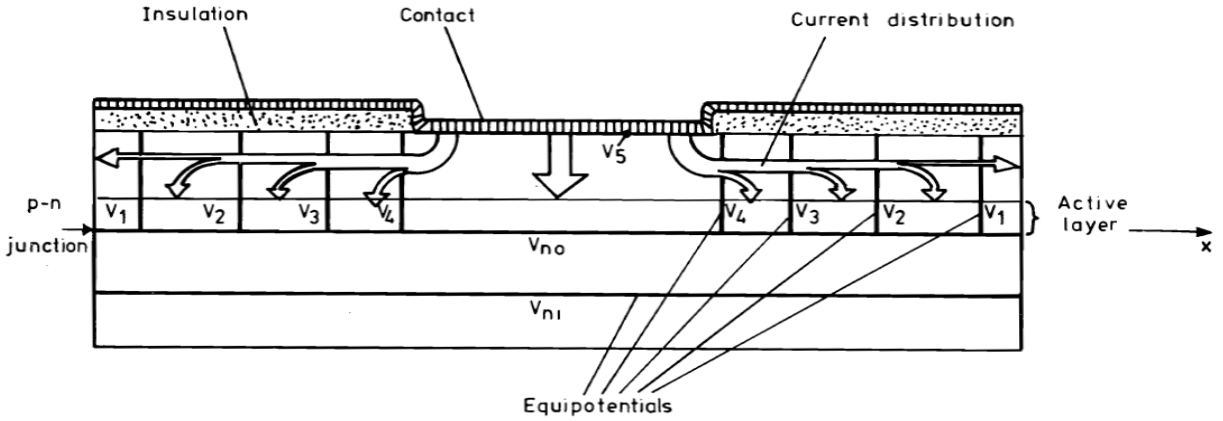

Figure 3: Model for striped laser used by Thompson

$$\frac{d^2V(z)}{dz^2} = \frac{\rho j_0 e^{\frac{qV(z)}{kT}}}{W}$$

Equation 1: Differential Equation used by Fletcher.[54].

The work by Thompson showed a precipitous drop in current from the edge of the strip to the end of the device. It was shown that the extent of current spreading seen in the device was highly dependent on the conductivity of both the shell and the core of the device[1]. More recently, work has been done on the GaN mesa LED structure by Guo et. al. the

current crowding underneath a contact covering the entire p-type region of a GaN mesa LED was examined to determine current crowding effects in this structure[51]. The electrode used in Guo's work fully conformed to the p-type mesa structure making this model inapplicable in this work. However, similar conclusions were made in this work, relating the conductivity of the n and p-type sides of the device to the extent of current spreading in the device.

Current Crowding and Device Efficiency

Equation 1 can be used to model the current crowding in a device with constant core doping. However, this model was derived by making the assumption that one side of the device (in this case the n-doped base) was uniformly highly doped and therefore presented an equipotential region . In the situation of a core-shell nanowire with a non-conformal shell electrode and non-uniform doping both of these assumptions are inaccurate, however, by neglecting any non-constant voltage in the core of the device, some judgments can be made regarding the causes of a non-constant junction voltage in the core-shell nanowire. If the model initially used by Fletcher and later by Thompson, which resembles the core-shell nanowire structure in two-dimensions, is examined, the current crowding in the uniformly doped core case can be calculated without loss of generality beyond the initial simplifications by Fletcher (this is discussed in Appendix A). In the case of non-uniform doping one must rely on simulation in order to come to any conclusions concerning methods of current crowding mitigation. This is due to the insertion of a non-constant resistivity into Fletcher's original equation for the second derivative of junction voltage (Eq. 1).

While current crowding is an issue that affects efficiency, the effect of a modified core doping profile is assumed to have only a specific range of applicability. Application

of the doping profile will reduce the doping concentration in some areas of the core of the device. This will have the effect of reducing the core conductivity. While it may affect the current crowding in the device it will also affect the total current allowed through the device. The radiative recombination which occurs in the device will be directly related to the current flowing through the device, so total radiative recombination will be reduced. The balance that needs to be struck is the largest conductivity in the core of the device constrained by efficient (uniform) distribution of current along the junction. Also, by changing the doping of the core of this device, the operation of the junction will be changed. This will result in different IV characteristics between different designs. To compare two different designs a method of analysis must be performed which takes these changes into account. A major problem with a junction design as large as that in a core-shell nanowire junction is that when the junction "turns-on" it can't be assumed that the entire junction is passing a constant current density or at a constant voltage, as was alluded to in the previous subsection. One possible way of taking this into account is keeping the minimum of the junction voltage the same between designs that are being compared. While they may not have the same area of the junction passing the same current density, this insures that the maximum current density being passed across one point of the junction is the same. The minimum of the junction voltage is a good proxy for the current flow across the device, because the current flow in the device will end up distributing across the junction in such a way that maintaining the minimum junction voltage at the same voltage is effectively the same as keeping total current into the device the same between designs. Further, the efficiency of the device over the entire region of operation will be the best measure of a successful design and will reveal which doping profiles have the best effect on overall device operation, rather than the highest direct recombination concentration at a single point.

Simulation of Current Crowding in Core-Shell Nanowires

Current crowding within this device structure is more complicated than the current crowding dealt with by Guo or Thompson. By performing a simulation over different designs and monitoring the junction voltage, a correlation between the doping profile and the current crowding within the device can be determined. Simulation of semiconductor devices can be accomplished through a variety of techniques, but one technique for steady state solutions to partial differential equations describing carrier and current densities in semiconductors is the finite element method. In the finite element method the system is divided into many surfaces (in 2 dimensions) or volumes (in 3 dimensions) within which conditions are assumed to be constant. Through coupled solution of the partial differential equations confined to these finite areas a solution for the entire system can be built up. For semiconductor devices the choice of partial differential equations to be solved in the finite elements are the drift-diffusion equations and Poisson's equation (Eq. 6). The simulator used is the TiberCAD multiphysics simulator[55]. This simulator provides a solver for drift-diffusion over a finite element grid. Advanced models for mobility and recombination are provided, and a large material database allows for modification of key material properties.

$$\vec{J}n = qn\mu_n\vec{\mathcal{E}} + qD_n\vec{\nabla}\mathrm{n}$$

$$\vec{J}p = qp\mu_p\vec{\mathcal{E}} - qD_p\vec{\nabla}p$$

$$\vec{\nabla}^2\varphi = \frac{\rho}{\mathcal{E}}$$

Equation 2: Drift-Diffusion and Poisson's Equation Solved by TiberCAD

The grid used in the finite element method defines the regions and boundary conditions used by the partial differential equation solvers. When using a discrete grid for simulation, the introduction of error due to improper grid spacing must be addressed. The finite elements must be given dimensions such that all variable and parameter changes that occur within each element are small. However, if the grid size is chosen too

small, the time taken by the simulation can be unnecessarily prolonged. Finding a proper compromise on grid sizing requires the use of system knowledge and awareness of data errors. In the case of a core-shell nanowire the route the current takes and the areas with large changes in carrier concentration are the key factors in determining grid spacing. In this structure the current should travel up the shell, cross the junction in to the core, and then continue to the contact on the core. The recombination events in this device should predominantly follow the current distribution within the device, and be highly concentrated at the junction of the shell and the core. This means that the grid refinement should be increased along the junction, but on the edge of the shell the grid size is not as important. TiberCAD allows for a grid with non-uniform grid spacing. This has been taken advantage of and a small grid size has been used along the junction, which linearly decreases to the edge of the shell and to the center of the core of the device.

The doping in the core is defined by creating spatially discrete steps in the doping of the core of the device. The doping steps must be defined so as to not result in long simulation times, but to provide a correct simulation of the effects of a variable doping profile. For most simulations, the doping profile will only be applied to the axial portion of the core of the device in direct contact with the shell. The portion of the core not in contact with the shell will be doped with the highest doping concentration in these cases. Later, to determine effects of doping profiles which extend into the core region with no direct contact to the shell, this will be changed. The doping profiles applied are based on a generating function which has a single parameter(Eq. 4), examples of doping profiles generated by this function are in figure 5[56]. The single parameter can be changed to create a variety of different doping profiles.

$$N_D(\alpha, z) = a_i + (a_i - a_0)(\left(1 - \left(\frac{z}{L}\right)\right)^{\alpha} - 1)$$

Equation 3: Doping profile generating function[56]

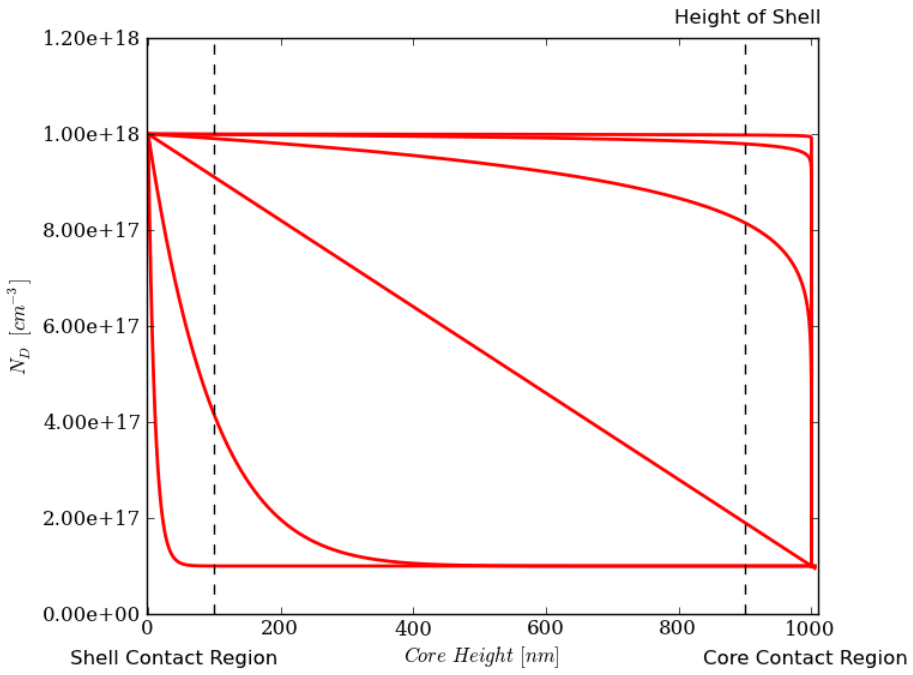

Figure 4: Doping profiles generated by the generating function

By varying the α term in the doping profile applied can be changed from an exponentially increasing dopant concentration along the axial coordinate, to a logarithmically decreasing dopant concentration along the axial coordinate. Also, the doping directions can be reversed to cover a large range of possible doping profiles.

The TiberCAD multiphysics simulator allows for a large database of materials parameters to be used in device simulation. In order to have an accurate simulation of gallium nitride nanowire devices, experimentally based data should be used to firmly base the simulation in reality. Of primary concern in this work are the effects of doping concentration and the effects of defects on recombination in GaN. The energy gap and the radiative recombination relations are the most basic parameters and have been known for quite some time[57]. Any effects of donor dopant concentration in the nanowire system also have to be taken into account, such as band gap narrowing[58], increased defects[32], or mobility effects[30]. The acceptor dopant concentration effects are important in simulating gallium nitride devices as the typical dopant concentrations

needed to provide usable acceptors need to be relatively large. This leads to mobility effects which may be taken into account[25, 26, 59].

Table 1: Primary Simulation Parameters

Parameter	Value
Electron Mobility	1500 cm^2/Vs
Hole Mobility	200 cm^2/Vs
Highest p-type doping	$1x10^{17}$ cm^{-3}
Highest n-type doping	$1x10^{18}$ cm^{-3}
Lowest n-type doping	$1x10^{17}$ cm^{-3}
Mobility Doping Dependence	Constant
Radiative Recombination Constant	0.47 s^{-1}

CHAPTER 5

SIMULATED CURRENT CROWDING

The current crowding in the device was simulated using TiberCAD as outlined in the previous sections. The current crowding was compared at different bias points which correspond to identical minimum junction voltages, which translates into very similar total currents. While this does not guarantee the entire junction is in the same state, something we cannot enforce, it does guarantee the point of maximum concentration of current across the junction will be the same, and the device will be in a similar operating regime across designs.

Initial Constant Core Doping

In the initial simulations a core-shell nanowire with a constant core doping of $1x10^{18}$ cm^{-3} is used. The effects seen in this device are purely due to the geometry of the device and the inequality of conductivity between the core and shell of the device. The current density normal to the junction is shown with a vector plot of current in Figure 6. Significant current crowding is clearly observed. A 3-dimensional plot of the conduction band surface is shown with the direct recombination concentration overlaid on top of the surface in Fig. 7). This device is at an applied bias of 3.2 Volts. Direct recombination can be observed in a high concentration below the contact on the shell. From the conduction band it is clear the electron density is highly concentrated at the lowest part of the core (near the shell contact). This provides an explanation for the high concentration of direct recombination in the lower section of the nanowire device. In the figure of the junction voltage the junction voltage (Fig. 8) and the current density (Fig. 6) agree in that the decreased junction potential barrier (junction voltage amplitude) occurs in the areas with highest current density. In the portion of the device closest to the shell contact there is a low junction voltage, which relates to a high current density across this region.

However, the junction voltage increases with z-coordinate in the device, corresponding to reduced current density and direct recombination in the device. Eventually another reduction in the junction voltage is seen near the core contact where there is another region of increased current density and direct recombination.

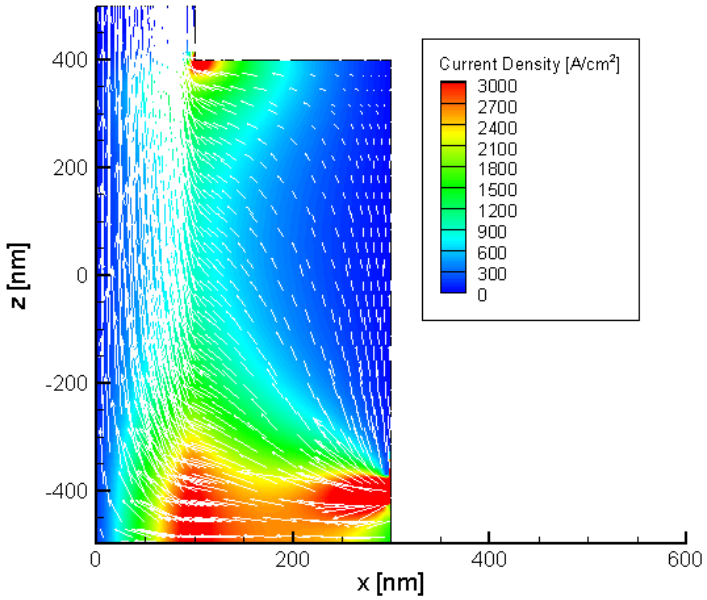

Figure 5: Current Distribution in Constant Doped Case

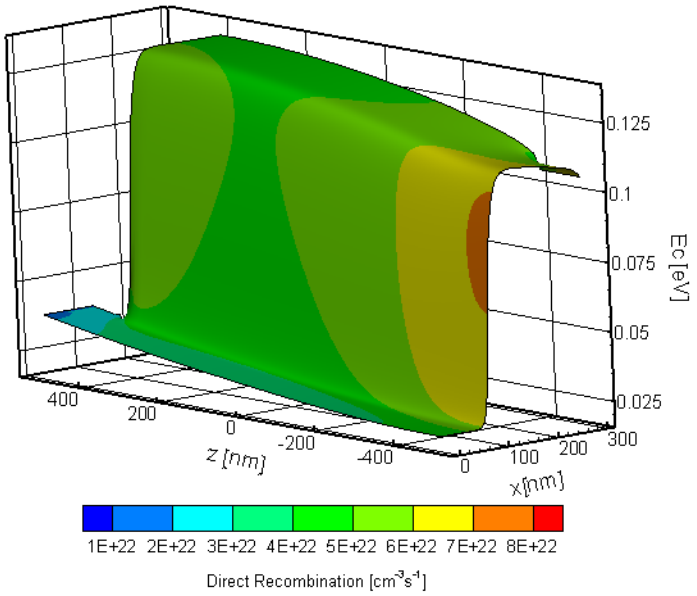

Figure 6: Conduction band with direct recombination overlaid in Constant Doped Case

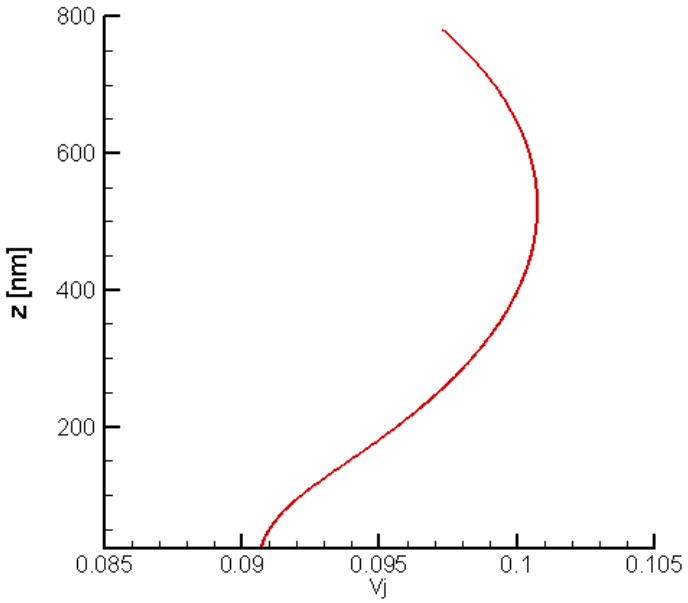

Figure 7: Junction voltage as a function of junction axial position z in constant doping case.

Core Doping With Increased Doping in the Shell Contact Region

Alpha 0.001

In the first doping profile a value of $\alpha = 0.001$ is used in the trial doping function generator. The doping profile in this case is shown in figure 9. The current density normal to the junction is spread out more evenly, resulting in a reduction of current concentration across the device, but tends to concentrate near the core contact region where the shell of the device stops (Fig. 10). The 3D plot of the conduction band reveals a deviation in the core conduction band due to the reduced doping seen at the edge of where the shell of the nanowire stops (Fig. 11). This deviation is due to keeping the core doping of the top of the device constant while applying the doping profiles only to the region of the core which is in contact with the shell. The junction voltage in the shell contact region of the device is more uniform than that of the constant doped device (Fig. 12). Except in the region at the edge of the shell, this is most likely due to the deviation created in the conduction band creating a region of the junction barrier that is slightly easier for current to overcome.

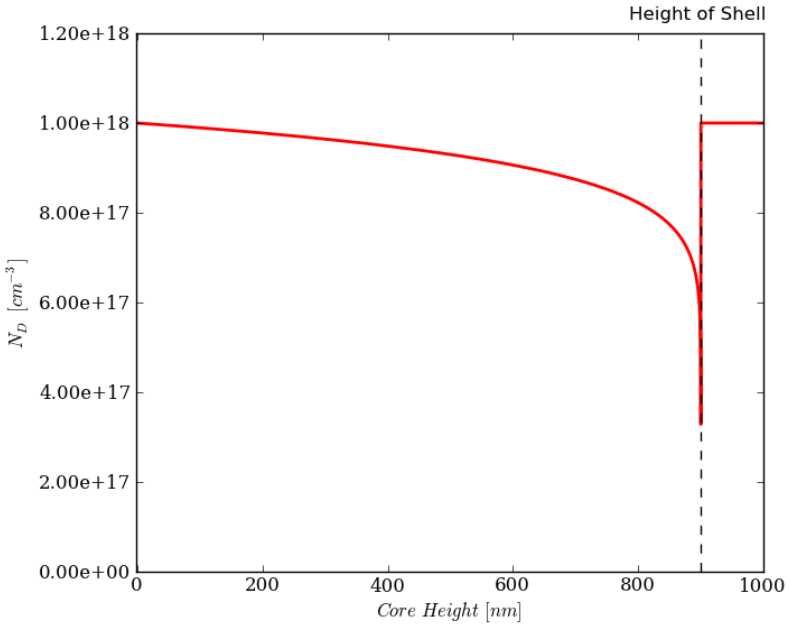

Figure 8: Doping in Alpha 0.001 with high doping in the shell contact region

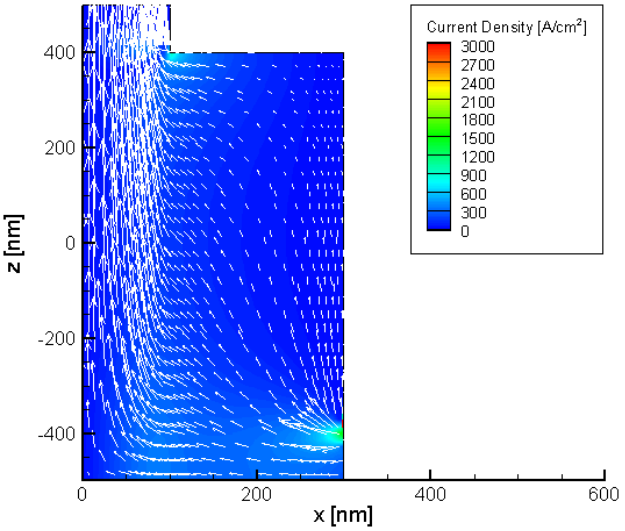

Figure 9: Current Distribution In Alpha 0.001 high doping in the shell contact region

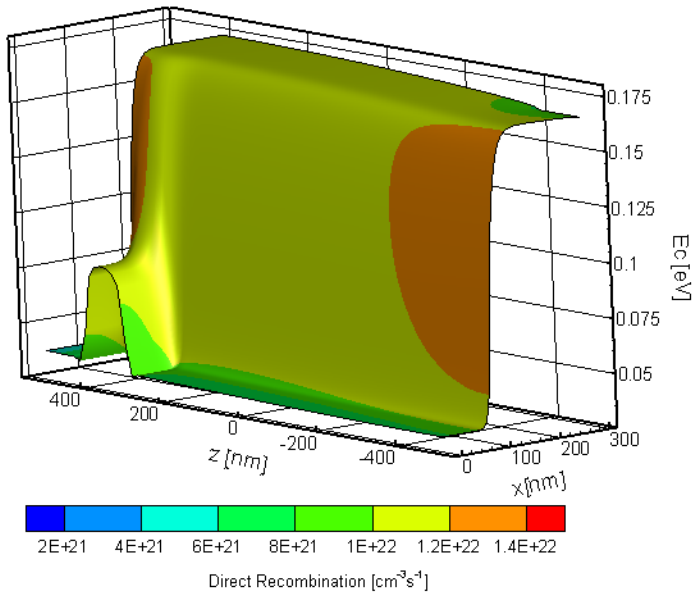

Figure 10: Conduction Band with Direct Recombination overlaid in Alpha 0.001 high doping in the shell contact region

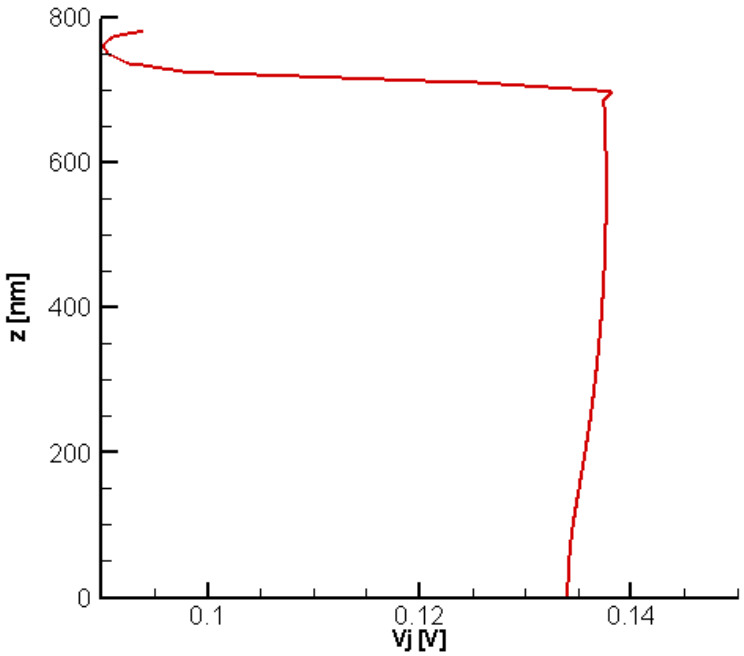

Figure 11: Junction voltage in alpha 0.001 with high doping in shell contact region

Alpha 1

With a doping profile provided by the trial doping function with an alpha value of 1 a linearly increasing doping profile is applied as a function of the axial z-coordinate within the device. With the linear doping profile (Fig. 12) a more uniform distribution of current (Fig. 13) and direct recombination (Fig. 14) occurs than in the constant core doped case. The shallowest junction potential resides nearest to the core contact, presumably due to decreased doping in the core region nearest the core contact. . The junction voltage along the height of the nanowire (Fig. 15) is consistent with the direct recombination (Fig. 14) and current distribution (Fig. 13) within the device.

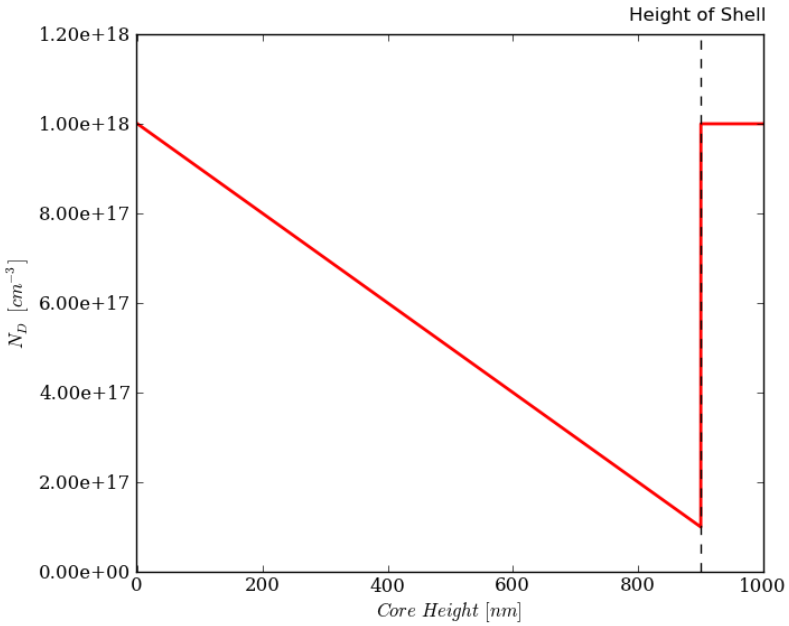

Figure 12: Doping in Alpha 1 with high doping in the shell contact region

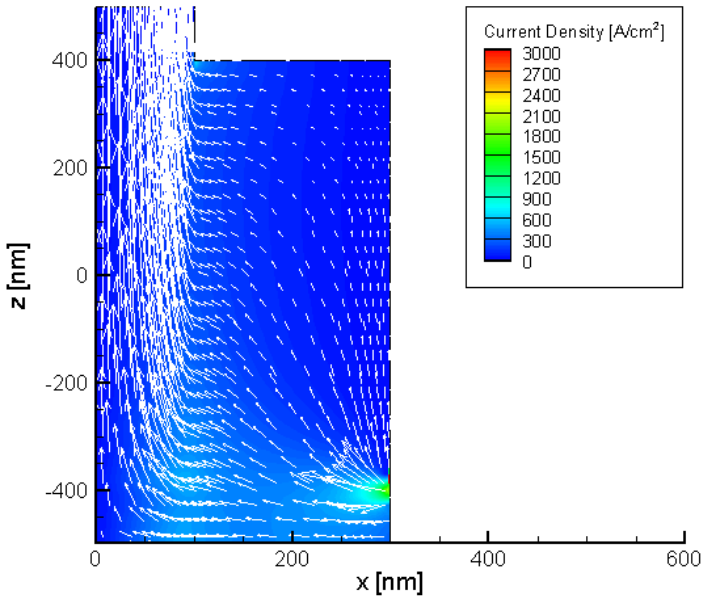

Figure 13: Current Distribution In Alpha 1 high doping in the shell contact region

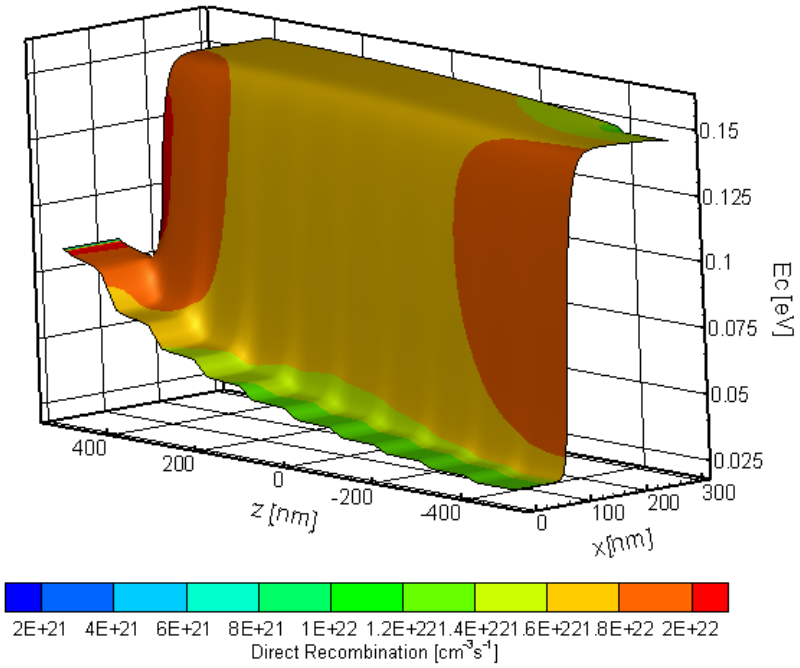

Figure 14: Conduction band with direct recombination overlaid in Alpha 1 high doping in the shell contact region

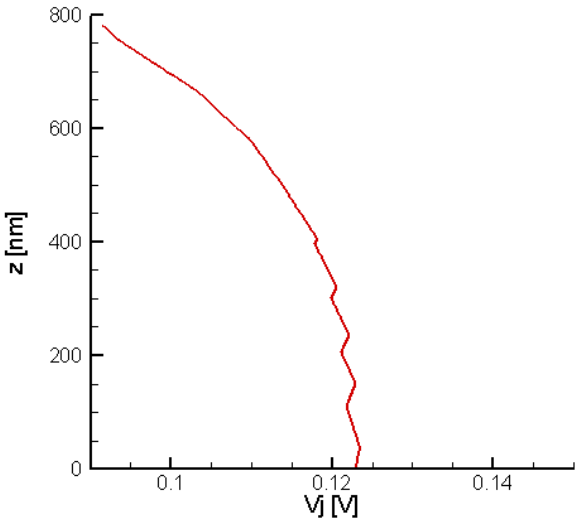

Figure 15: Junction voltage in alpha 1 with high doping in shell contact region

Alpha 100

With a trial doping function created by α = 100 the doping profile is predominantly low doped except for a region of increased doping near the shell contact area of the device (Fig. 16). The increase in doping near the core contact of the device is again due to constraining the core region of the device not in contact with the shell to have a uniform doping. The distribution of current in this case is concentrated near the core contact of the device (Fig. 17). The conduction band diagram (Fig. 18) and the junction voltage plot (Fig. 19) reveal there is an increased barrier to current flow in the region directly beneath the shell contact, due to increased junction voltage. From the current density diagram (Fig. 17) the effect on current crowding within the device is fairly drastic. However the peak current density is also reduced most likely due to reduced conductivity in the core of the device.

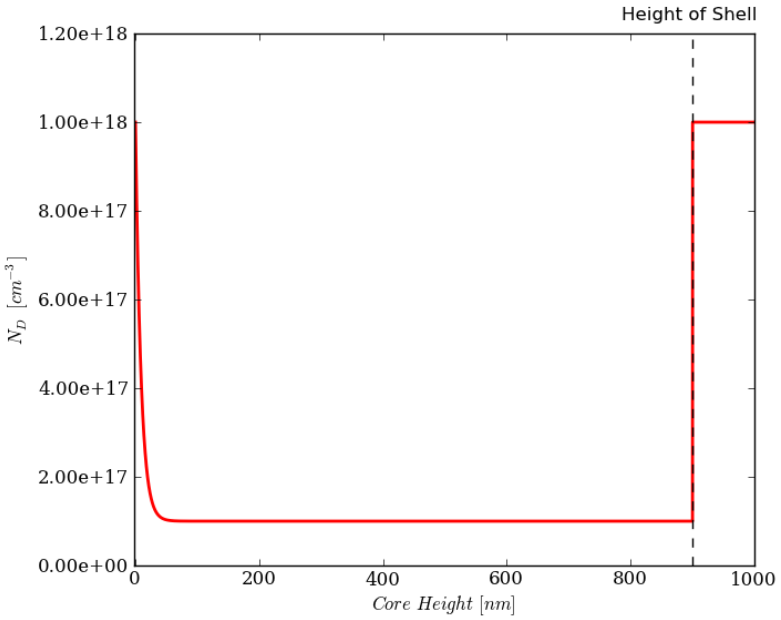

Figure 16: Doping in Alpha 100 with high doping in the shell contact region

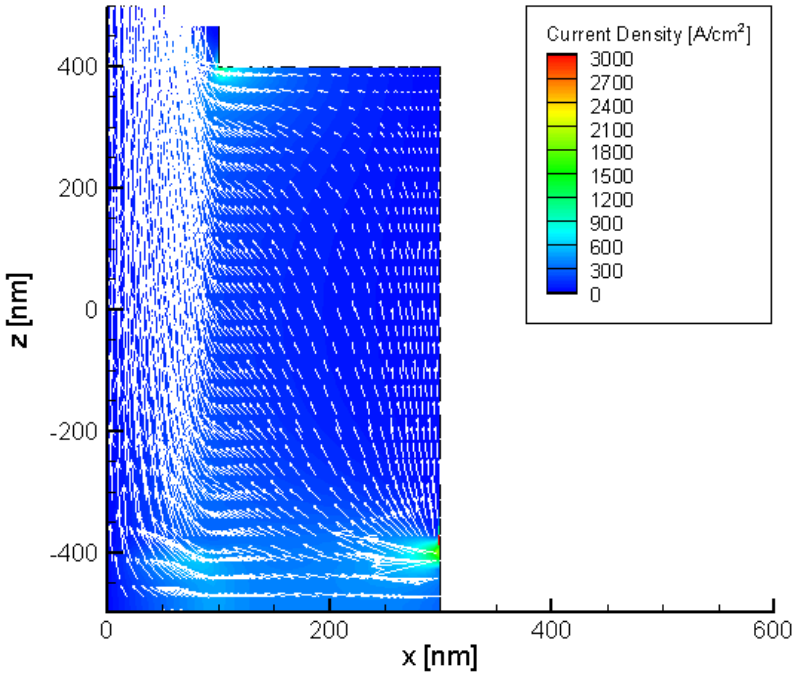

Figure 17: Current Distribution In Alpha 100 high doping in the shell contact region

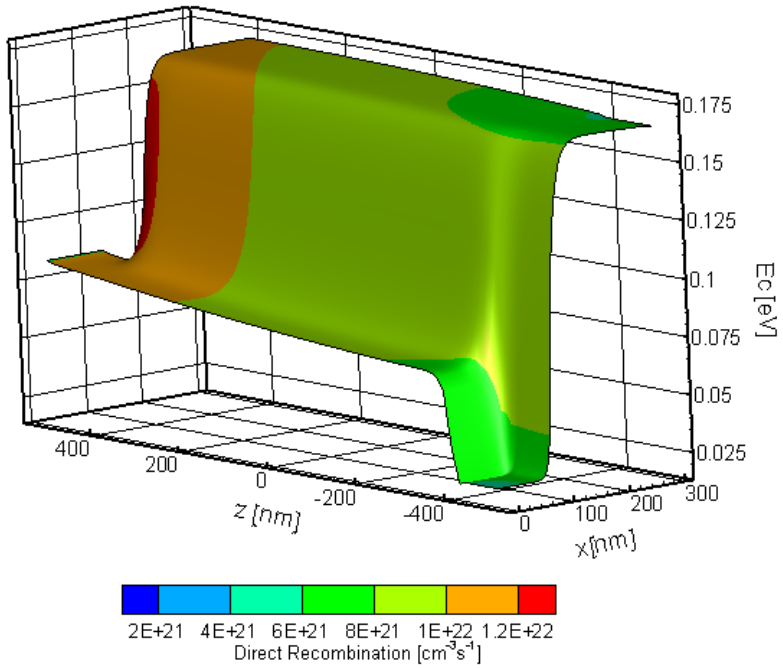

Figure 18: Conduction band with direct recombination overlaid in Alpha 100 high doping in the shell contact region

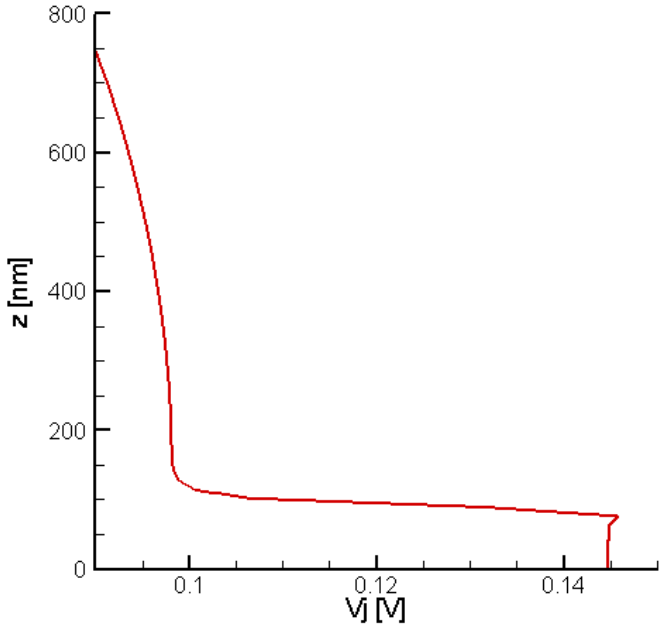

Figure 19: Junction voltage in alpha 100 with high doping in shell contact region

Core Doping with Increased Doping in the Core Contact Region

Alpha 0.001

In the case of a doping profile where $\alpha = 0.001$ there is an increased dopant concentration in the core contact region (Fig. 20). The current density distribution (Fig. 21) and direct recombination (Fig. 22) include a heightened concentration of current and direct recombination respectively in the region of increased dopant concentration. Even with increased direct recombination and current density near the core contact region of the device current crowding is reduced and the direct recombination forms a more uniform distribution, with a reduced peak compared to the constant doped case. The junction voltage (Fig. 23) also reflects this effect with reduced junction voltage amplitude in the region nearest the core contact.

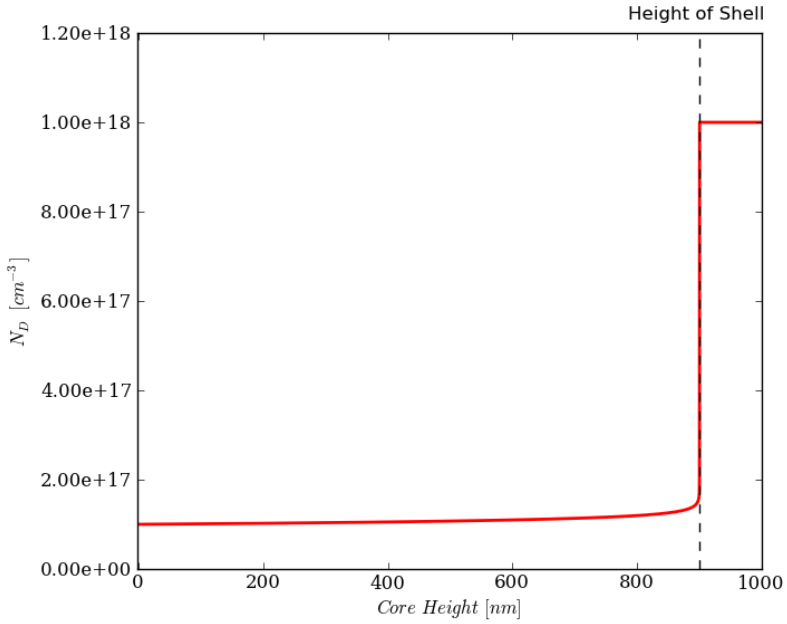

Figure 20: Doping in Alpha 0.001 with high doping in the core contact region

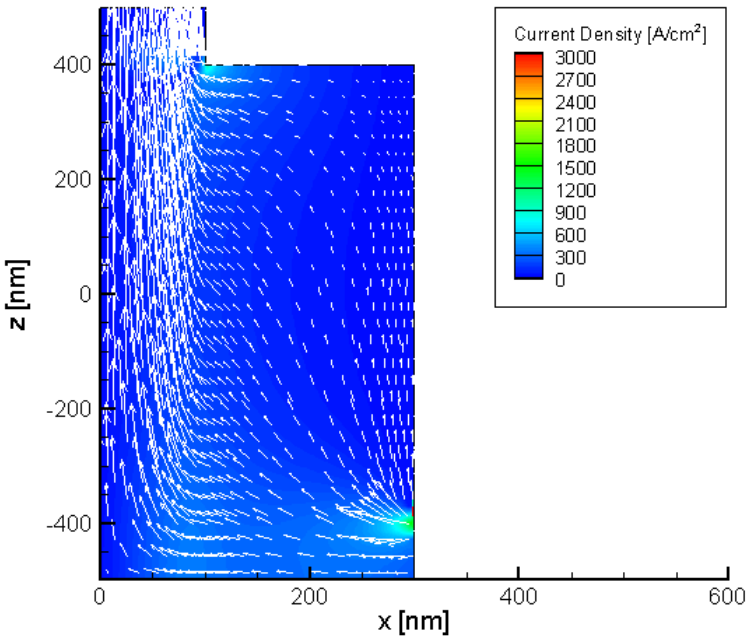

Figure 21: Current Distribution In Alpha 0.001 high doping in the core contact region

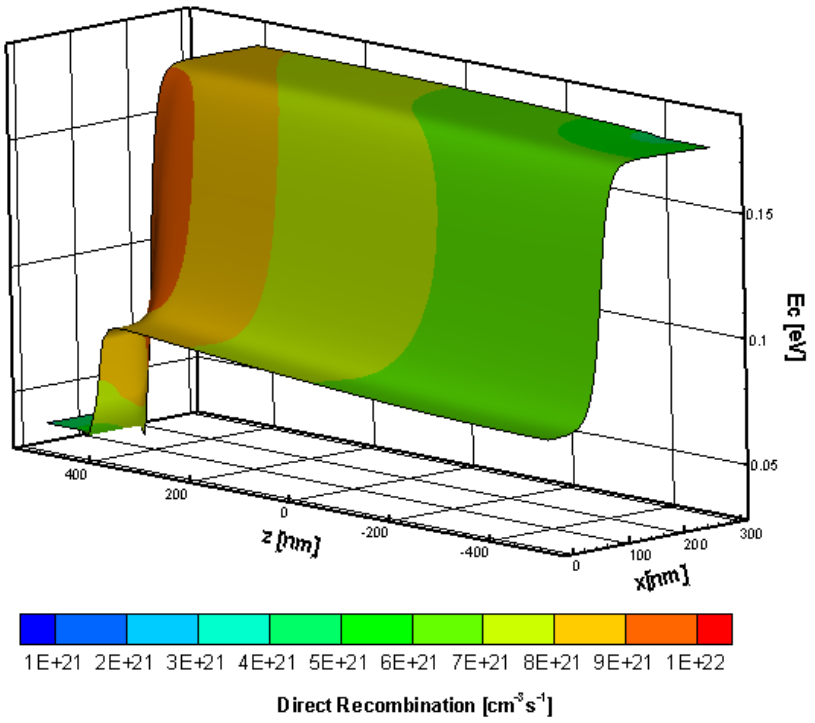

Figure 22: Conduction band with direct recombination overlaid in Alpha 0.001 high doping in the core contact region

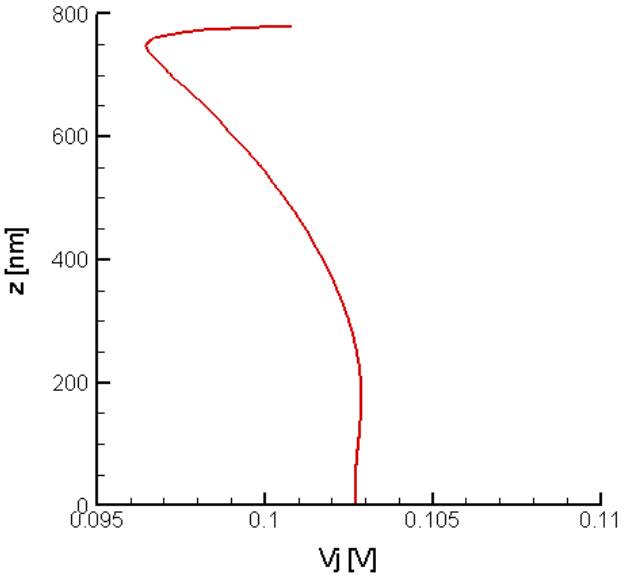

Figure 23: Junction voltage in alpha 0.001 with high doping in core contact region

Alpha 1

A linear doping profile with increased dopant concentration in the core contact region (α = 0.001) is shown in Figure 24. Application of this profile leads to some current crowding around the shell contact edge (Fig. 25), and increased direct recombination concentration in the area of the shell contact of the device (Fig. 26). As the doping has been reduced in the shell contact region the barrier is reduced (Fig. 26). The reduction of the barrier height can be seen in the junction voltage (Fig. 27). This reduction in barrier height causes a large concentration of current to flow across the junction beneath the shell contact, however when compared to the constant doping case the extent of this concentration has been reduced, resulting in a device with reduced current crowding effects, most likely due to both reduced conductivity in the core region and a change in the barrier changing the path of least resistance through the device.

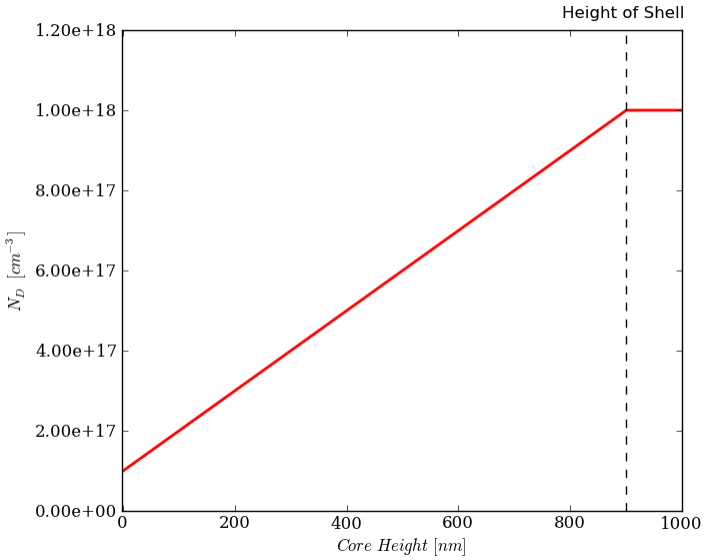

Figure 24: Doping in Alpha 1 with high doping in the core contact region

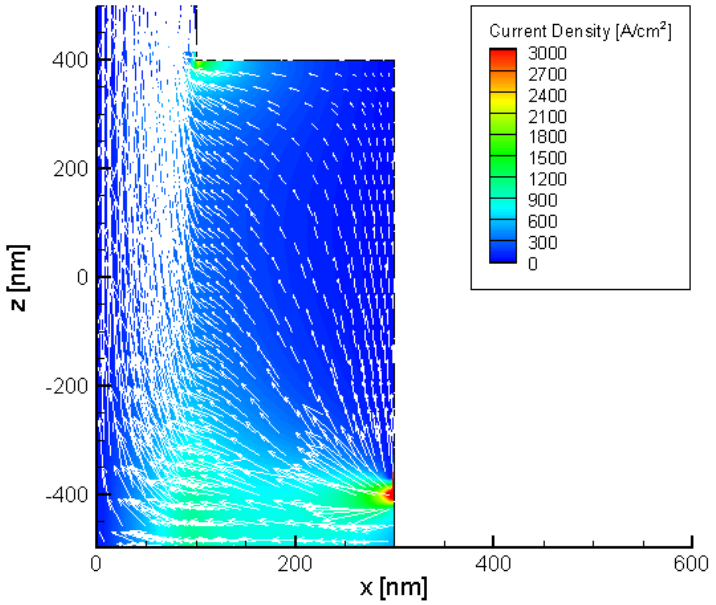

Figure 25: Current Distribution In Alpha 1 high doping in the core contact region

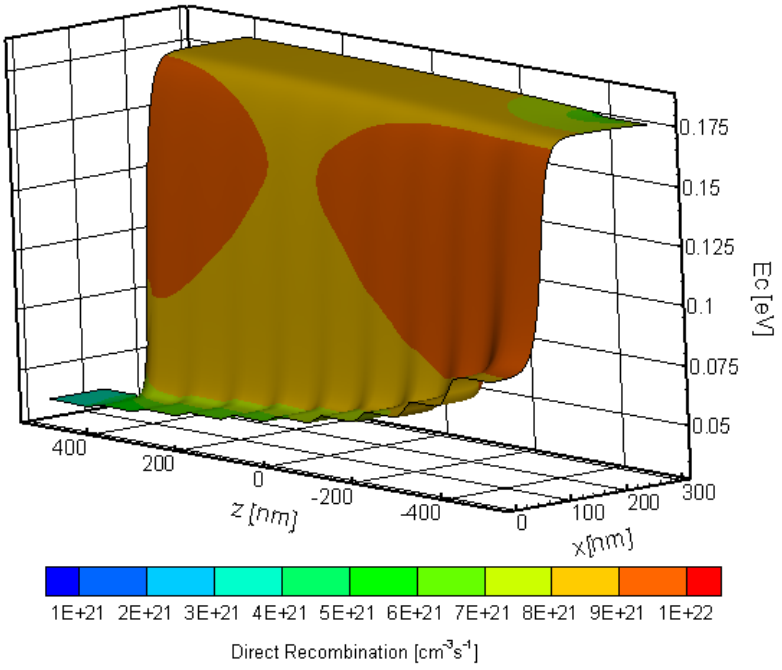

Figure 26: Conduction band with direct recombination overlaid in Alpha 1 high doping in the core contact region

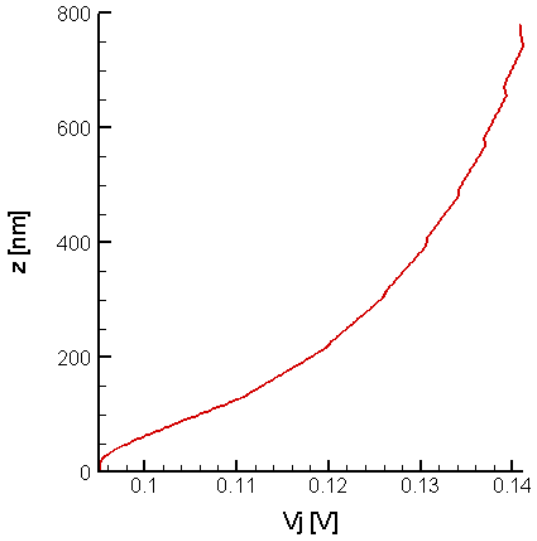

Figure 27: Junction voltage in alpha 1 with high doping in core contact region

Alpha 100

For a doping profile α =100 the highest region of doping occurs in the core contact area (Fig. 28). The increased current flow directly beneath the shell contact of the device is evident in the current diagram (Fig. 29) and can be inferred from the increased concentration of direct recombination (Fig. 30). The barrier at the junction in this case has been reduced in the region just behind the shell contact, while the conductivity has remained high, which can be seen in the plot of the conduction band (Fig. 30). The plot of the junction voltage follows that of the conduction band plot, revealing a small junction barrier in the shell contact region followed by a relatively constant junction barrier for the rest of the device (Fig. 31).

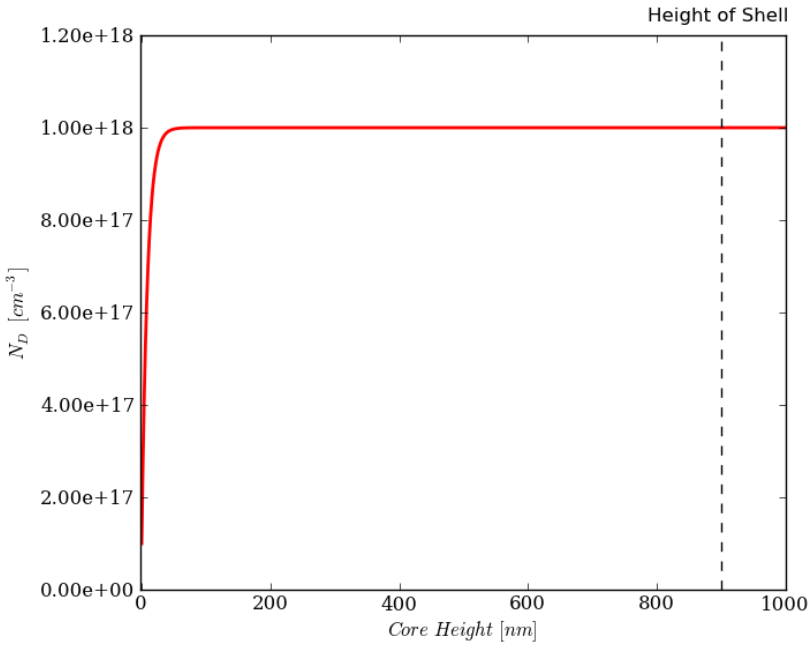

Figure 28: Doping in Alpha 100 with high doping in the core contact region

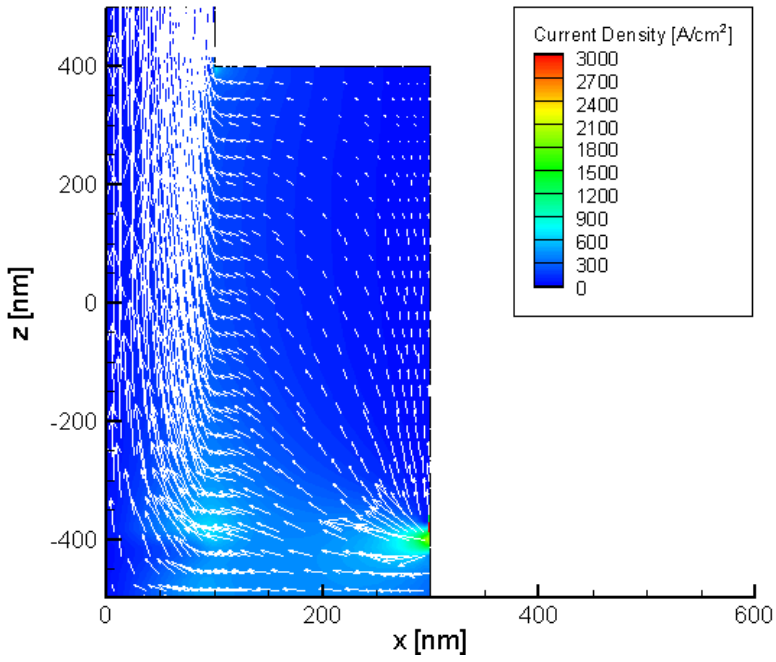

Figure 29: Current Distribution In Alpha 100 high doping in the core contact region

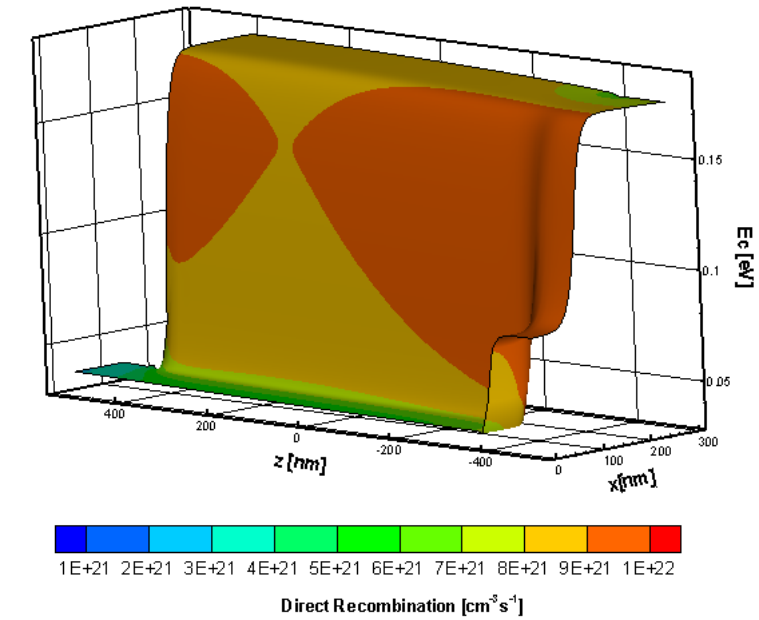

Figure 30: Conduction band with direct recombination overlaid in Alpha 100 high doping in the core contact region

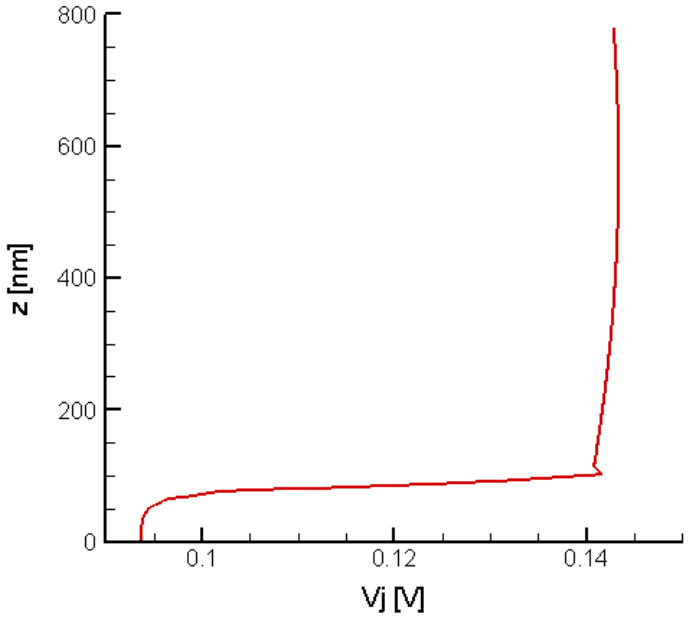

Figure 31: Junction voltage in alpha 100 with high dopant concentration in core contact region

Extending Doping Into the Isolated Core

To this point the doping profile has only been applied to the core where the shell is in direct contact. The core which extends past the shell of the device should only affect the total current allowed into the device and this should have little effect on the device efficiency. This has provided some promising results; however, the model and optimization developed in appendix A suggest that the total current and the derivative of the core resistivity may have an effect on the current crowding in this device. The effects of a non-constant doping profile extended into the core region beyond the shell of the device will briefly be covered to investigate promising behavior. The doping profiles with low dopant concentrations near the core contact appeared to create the most current spreading within the device. Of these doping profiles, the most effective is the device with $\alpha = 0.001$. By reducing the doping into the core not in contact with the shell (above 900 nm where the shell ends) (Fig. 32) the current concentration is spread in a more uniform fashion than any of the other doping profiles as is evident from Figure 33. The direct recombination (Fig. 34) is uniform across the device in response to the evenly spread current. Finally, the junction voltage has a shape similar to the constant doped case, but the magnitude of the junction voltage change is reduced (Fig. 35). A reduced change in the junction voltage (with height) should come with an increased spread of current across the device. This is the case in this situation as is seen in Figure 33.

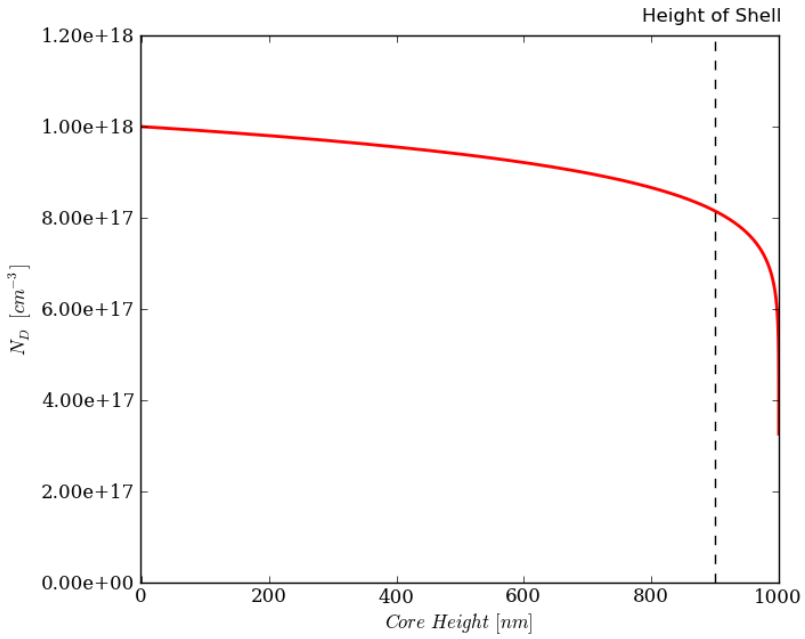

Figure 32: Doping Diagram of Device with profile extended into core region above shell

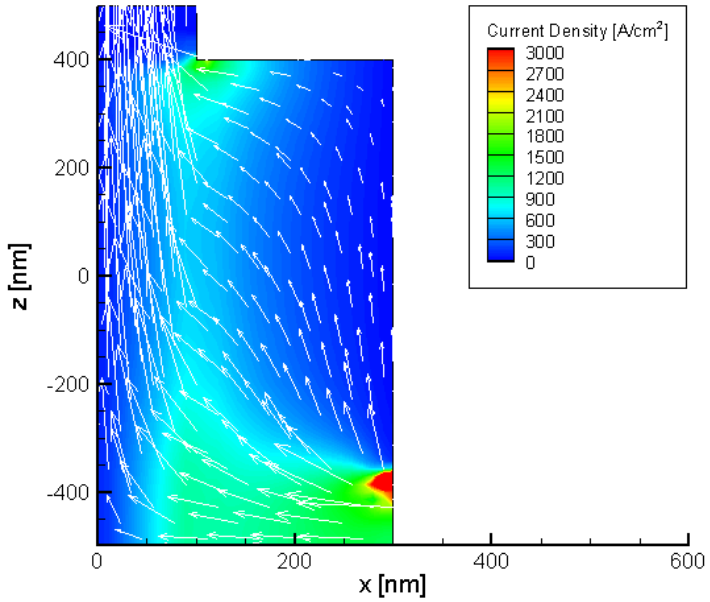

Figure 33: Current Density in alpha 0.001 with doping profile extended into core beyond shell

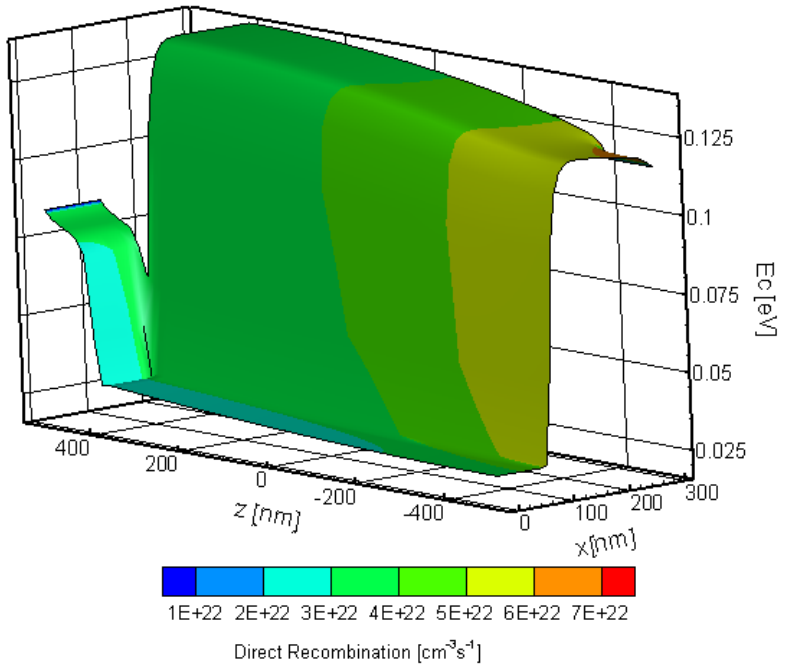

Figure 34: Conduction band with direct recombination overlaid in Alpha 0.001 high doping in the core contact region with doping profile extended beyond shell

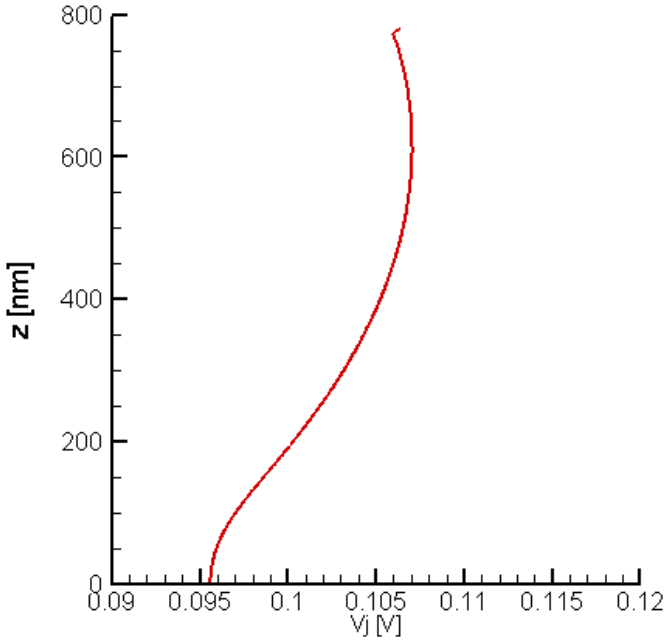

Figure 35: Junction voltage in alpha 0.001 with high doping in core contact region, with the profile extended beyond the shell

Summary of Results

The application of almost all of the doping profiles attempted in this study had some beneficial effects on current crowding and direct recombination distribution. However, in all cases the peak direct recombination in the simulation was reduced relative to the constant doped case. This isn't necessarily undesirable , if the efficiency of light production is increased while having a reduced peak radiative recombination the device can arguably be better for application as an LED. Furthermore, the peak radiative recombination in the constant doped simulation occurs directly behind the shell contact. If an opaque contact is used, then the light emitted in this area would be drastically reduced by absorption. As current crowding has been shown to be reduced by changing the way the core of the nanowire is doped, what remains to be seen is if this actually increases the operational efficiency of the device. The most interesting device structure in this case is the doping profile which was extended into the core of the device above the shell. As this method is at first somewhat counterintuitive, it does provide a glimpse into what actually influences current crowding within the core-shell nanowire structure.

CHAPTER 6

SIMULATED EFFICIENCY

In a p-n junction device without quantum wells, recombination is generally greatest within a diffusion length of the depletion region of the device due to the joint electron and hole densities . This can typically be used to define an area with which to estimate the efficiency of LED structures. However, the small size of the core-shell nanowire is prone to full depletion. The depletion region in the core-shell nanowire can extend relatively far into the shell of the device simply because the device has a small diameter. Careful consideration of the manner in which efficiency is calculated must be done . Due to the sensitivity of the depletion region, the applied bias in the device must be carefully controlled. Further, the changes in the barrier height and material conductivity modify the intrinsic operation of the p-n junction. The "turn-on" voltage of the device is the primary concern, as was discussed in the previous section. In this section it is important to make a distinction between LED operation after turn-on of the p-n junction and operation at the flat-band condition. In the flat-band condition, the depletion region in this core-shell device has spread far into the shell and core of the core-shell nanowire. Also, at this point there is no potential barrier at the junction, and current through the device is limited by the conductivity and high field effects only, and therefore the recombination simulated at this point is dubious. The analysis of current crowding using the methods in this work is not applicable to this case. . This issue can be resolved by only looking at the efficiency of the device in a window of operation between initial turn-on and when the flat-band condition begins to take effect. Within these limits, we compare the efficiency of the device designs tested to determine the beneficial effects of non-constant doping. This section will look at the efficiency of the

different core doping profiles and compare these to the current crowding found in the previous section. For our purposes, we define efficiency as the total direct recombination integrated over the entire volume of the nanowire divided by input power (Eq. 4). This will provide a value that can be compared between designs.

$$\text{direct recombination efficiency} = \frac{\text{total direct recombination}}{\text{input power}}$$

Equation 4: Definition of Efficiency Used in This Work

High Doping in Shell Contact Region

The doping profile with the highest doping in the core contact region with an alpha value of 0.001 showed some reduction in current crowding within the core-shell nanowire device. This device shows an increase in the efficiency of the production of direct recombination in the device, as seen in Fig. 36. The efficiency is shown for a range of applied biases which are centered around the effective turn-on voltages of the devices. This provides evidence that the doping profiles leading to more efficient operation are actually increasing efficiency, and the devices are not merely being biased at different regions of their operation.

The efficiency seen in the case of linear doping shows a marginal increase in efficiency relative to the constant doped case, showing a similar flat efficiency region as seen in the constant doped case, which was notably absent from the case of a doping profile with alpha value of 0.001. The efficiency of the device with a doping profile marked by alpha value 100 is very close to the efficiency of the constant doped core device (Fig. 36). This device had fairly good current crowding control, but no improvement in efficiency compared to the constant core doped device; also, the region of reduced efficiency increase is more evident than in the linearly doped case.

The doping profiles in this set of data contain high dopant concentrations near the core contact region but contain reduced dopant concentrations in the shell contact region.

This causes a reduction in the barrier height in the shell contact regions, but also a reduction in core conductivity. The efficiency data for these doping profiles provides two routes to increased efficiency in radiative recombination production. A reduced dopant level in the in the core contact region can increase the efficiency of device operation. However, judging from the linear doping profile ($\alpha = 1$) some qualification is necessary. In the case of $\alpha = 0.001$, by decreasing the doping concentration in a very narrow area near the edge of the shell closest to the core contact(Fig. 8) a path of least resistance, made up of the conductivity of the core added to the effective resistance introduced by the barrier height can exist within the shell to the region of least junction height(the deviation introduced in the core side of the conduction band diagram in Figure 9). By looking at the junction voltage for this design (Fig. 11), one can see a significant change in junction voltage in the portion of the junction closest to the core contact. This can be attributed to the reduced junction height present in this region (Fig. 9) allowing a significant current drop in this region, which has the effect of reducing current crowding within the entire device by modifying the route of the path of least resistance. The profile in the case of $\alpha = 100$ decreases the doping in most of the core other than the area directly below the shell contact. This presents a reduced junction height in all areas of the junction other than directly beneath the shell contact. This effectively reduces the fitness of the typical path of least resistance through the device (current travels directly beneath the shell contact and up the core), by reducing the junction height of the rest of the junction, but also decreasing the conductivity of the path up the core of the device.

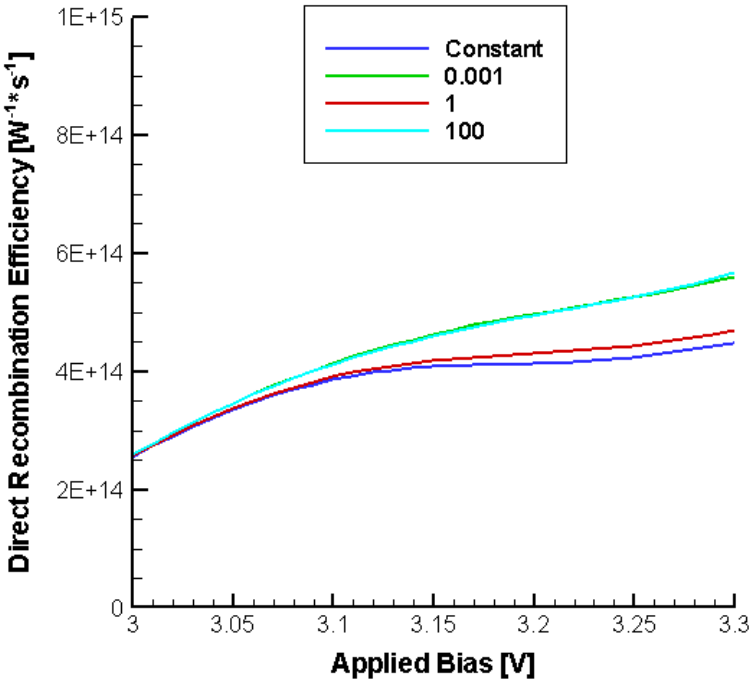

Figure 36: Calculated Efficiency for all cases with high doping in the shell contact region

High Doping in the Core Contact Region

The doping profile produced with a trial doping function with α=1 with high doping in the core contact region and linear doping profile produced a more uniform distribution of current along the junction than in the constant doped case, heuristically(Fig. 25). The efficiency (Fig. 37) shows only a marginal increase in efficiency than the constant doped case. The device with a doping profile with α=100 has a further increase in efficiency over the linear doped case. The current spreading in the device also appears more uniform (Fig. 29). Also, the junction voltage appears more uniform over a larger area of the junction (Fig. 31) than in the linear doped case and the doping with α=0.001. The efficiency increases can be attributed to similar reasons as in the previous section, where a combination of conductivity in the core and barrier height

can affect the path of least resistance through the device. In both cases by looking at the change in the junction voltage the devices with increased current spreading can be determined. These then tend to operate more efficiently than the constat doped case.

Notably, the efficiency of the device with the doping profile extended into the isolated portion of the core of the nanowire shows a remarkable efficiency increase. From this devices distribution of current (Fig. 33) this result can be understood as follows. Due to the doping profile applied, the current crowding has been sufficiently reduced across the device, as evidenced by the limited magnitude of change in the junction voltage in this device (Fig. 35). This limited current crowding allows for a more even distribution of carriers and thereby direct recombination across the junction of the device, as seen in Figure 34. The distribution of current in the device is a combination of core conductivity gradient and junction barrier height gradient which leads to a device with mitigated current crowding and thereby increased efficiency. The doping profile leading to this result is somewhat surprising in that it is a limited change to a region of the device not in contact with the shell, and also from basic semiconductor principles should only act to limit the total current through the nanowire. The efficiency of a device with a constant core doping of $1x10^{17}$ cm^{-3} has also been included in Figure 37 to show that optimization of the efficiency of these devices is not merely reliant on having reduced current or more equivalent doping concentrations in the p and n-type regions.

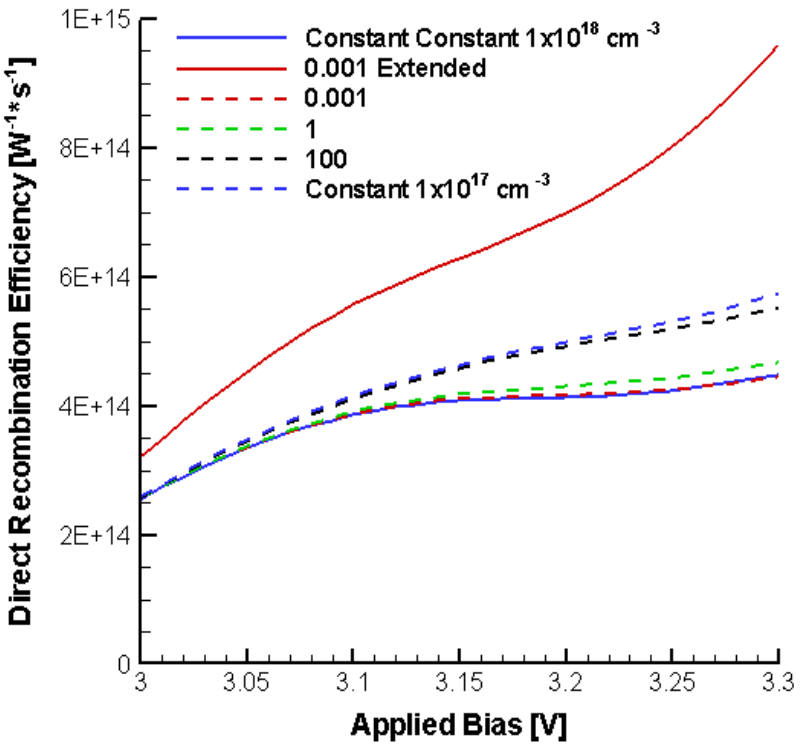

Figure 37: Calculated Efficiency for all cases with high dopant concentration in core contact region

Summary of Results

Although almost all the devices appeared to abate the problem of current crowding in this device, the effects on the efficiency of the device operation have been marginal in some cases despite the fact that the current was made more uniform than in the constant core doped nanowire. However, there were a few cases where efficiency was increased in a more than marginal amount, and in one case the efficiency was increased by around 60 percent. As expected, the general efficiency reflects the overall current crowding within the device, which can be related to the junction voltage. As the

junction voltage moves closer to a constant value with the height of the device the more evenly the current is spread and the higher the efficiency of the device.

Table 2: Efficiency Values at Similar Bias Points

Alpha Value	Efficiency at bias point
Constant Doping	4.13429E+014
High Doping in Core Contact Region	
0.001	4.9149E+014
1	4.20821E+014
100	4.50972E+014
High Doping in Shell Contact Region	
0.001	4.04392E+014
1	4.09924E+014
100	4.41115E+014
0.001 with doping profile extended into contact section	6.02055E+014

CHAPTER 7

CONCLUSIONS

The key to maintaining uniform current distribution is obtaining a constant junction voltage across the entire height of the core-shell nanowire junction. With the device geometry chosen for this analysis the task is made difficult by the low conductivity of p-type GaN. To counteract this, a set of doping profiles were applied to the core of the core-shell nanowire in an effort to create a more uniform junction voltage. It was found that several variations in the doping profile of the core of the device can produce a more constant junction voltage, however only some of these variations provide for more efficient operation. Of the doping profiles analyzed the most compelling doping profile in terms of increased efficiency, and reduced current crowding used a doping profile of the form of figure 32. This doping profile corresponds to the device with the junction voltage seen in figure 35. This doping configuration uses a narrow region of reduced doping in the core of the device closest to the core contact. This will decrease overall current flow through the device, but is possibly affecting the distribution of current in the device through the resistivity change introduced in the region of the device where the shell ends. Through the use of a simplified model and several test cases it has been shown that by introducing a non-constant doping profile in a core-shell nanowire the concentration of current along the junction can be spread more evenly than in a constant doped device.. The junction voltage has been shown to be a good heuristic measure of the concentration of current along the junction. The current spreading in the junction of the device has also been shown to relate to the efficiency of direct recombination within the device. This allows for current growth techniques to be used to create more efficient LED designs by varying the doping of the device. In particular in

the case designated by $\alpha=0.001$ with a doping profile that is extended into the portion of the core isolated from the shell (Fig. 32).

APPENDIX A

DERIVATION OF JUNCTION VOLTAGE MODEL

The work by Thompson assumed the n-type region of the device was highly conductive and the voltage did not change in this layer, the junction was assumed to act like an ideal diode, and the exponential term was assumed to be much greater than 1. The assumptions regarding the high conductivity of one layer allowed only one side of the junction to be considered when calculating the junction voltage as the other region could be considered an equipotential surface. In modeling the core-shell nanowire structure in the case of this work neither layer can be assumed to have a constant voltage when a drastic non-constant doping profile is applied. However, in the case of uniform doping, the potential can be assumed to be a constant with height (Fig. 39), The core in this figure can be assumed to have a constant potential, but when the core doping is modified this assumption is less valid.

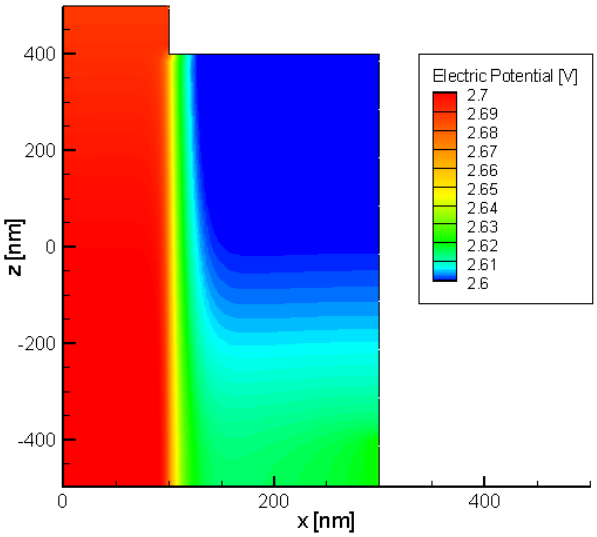

Figure 38: Constant core potential seen in Constant Doped Nanowire.

In the work by Fletcher, the junction voltage is assumed to be dependent on current crossing the junction multiplied by the resistivity seen in the core. (Eq. 5):

$$\frac{dV}{dz} = -\frac{\rho}{W} i(z)$$

Equation 5: Original Model By Fletcher

Where i(z) is the current across the junction at point z, ρ is the resistivity of the core, and W is the thickness of the core. In the coordinate system used by Fletcher, 0 is at the edge where the current is the largest (in the case of the nanowire it is at the edge of the shell contact closest to the core contact). The device is assumed to have zero current crossing the junction at infinity (the end of the junction furthest away from the shell contact in this case). Based on simulation this assumption is a somewhat inaccurate , but was used successfully by Thompson in modeling strip lasers, and the model still provides a coarse description of the major current crowding seen in the constant doped case . By taking the derivative of equation 5 given the current is the integral of the current density given by the ideal diode equation (Eq. 6), and assuming current at infinity is 0, the differential equation used by Fletcher can be found(Eq. 7).

$$i(z) = \int_z^{\infty} j_0 e^{\frac{qV(z)}{kT}} dz$$

Equation 6: Current across the junction at a point z[54]

$$\frac{d^2V(z)}{dz^2} = \frac{\rho j_0 e^{\frac{qV(z)}{kT}}}{W}$$

Equation 7: Differential Equation used by Fletcher.[54].

The solution to the constant case found by Fletcher (Eq. 7) for the voltage is given in equation 8.

$$V(z) \approx -\frac{2kT}{q} \ln\left[e^{-\frac{qV_0}{2kT}} \mp \frac{q}{2kT}\left(\sqrt{\frac{2\rho}{W} j_0 \frac{kT}{q}}\right) z\right]$$

Equation 8: Solution for the Constant Doping Case Originally found By Fletcher

When taken in the constant doping case the following is produced by the model with a electron concentration of $1x10^{18}$ cm^{-3} (taken from simulated data) in the core, with a core radius of 100 nm, the model is plotted with the simulation (Fig 39). The current crowding predicted by the model is evident from the potential values along the junction. As the core of the device is assumed constant the plotted potential is the magnitude of the potential referenced to ground on the shell portion of the device. The deviation between the model and simulation most likely come from the simplification made neglecting the -1 term from the ideal diode equation and from a non-ideal core potential. Both the model and simulation show an increased potential near the core contact (z=0), evidence of increased current crowding directly beneath the shell electrode. By inserting the expression for the junction voltage into the ideal diode equation the expression for the current density within the device can be determined (Eq. 9).

$$i(z) \approx j(0)\left[1 + z\sqrt{\frac{\rho q}{2WkT}j(0)}\right]^{-2}$$

Equation 9: Model for Current with Height of Device

The model for current (Fig. 40) resembles that from simulation in all areas but the current crossing the junction nearest to the core contact. This is presumably due to the assumption that the current in this region is zero. However, the current crowding in the region directly below the shell contact is evident from the model.

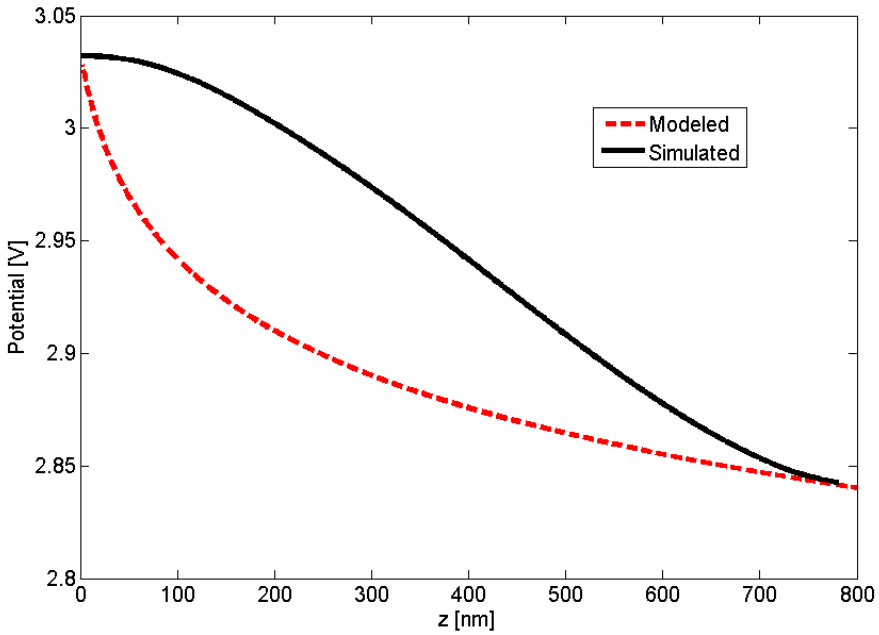

Figure 39: Comparison of Modeled and Simulated Junction Voltage

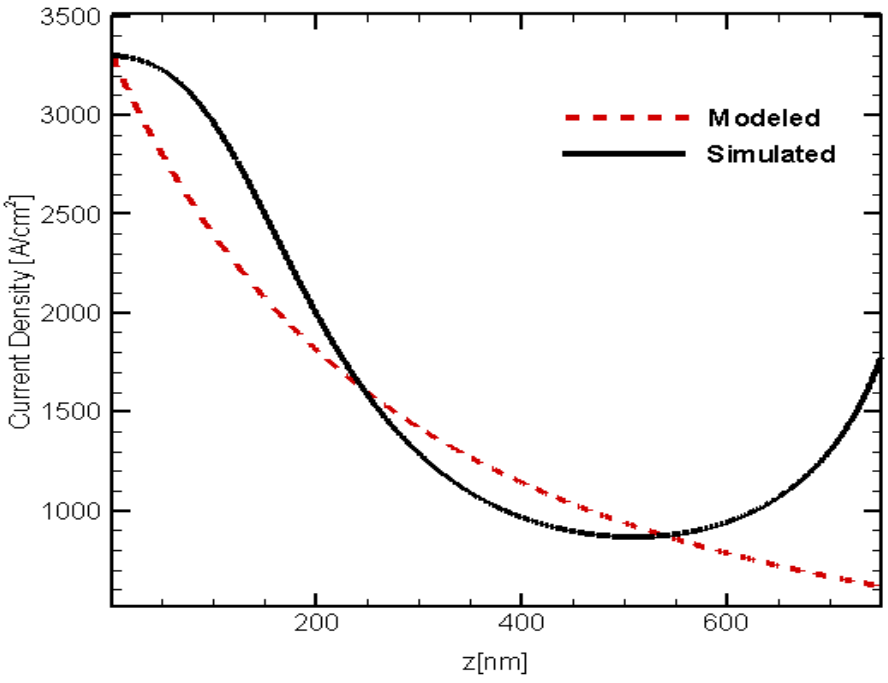

Figure 40: Comparison of Modeled and Simulated Junction Current Density

REFERENCES

[1] G. H. B. Thompson, *Physics of Semiconductor Laser Devices*, 1 ed. vol. 1. New York: John Wiley & Sons, 1980.

[2] M. Law, *et al.*, "SEMICONDUCTOR NANOWIRES AND NANOTUBES," *Annual Review of Materials Research*, vol. 34, pp. 83-122, 2004/08/04 2004.

[3] L. Geelhaar, *et al.*, "Axial and radial growth of Ni-induced GaN nanowires," *Applied Physics Letters*, vol. 91, pp. 093113-3, 2007.

[4] H. Y. Peng, *et al.*, "Bulk-quantity GaN nanowires synthesized from hot filament chemical vapor deposition," *Chemical Physics Letters*, vol. 327, pp. 263-270, 2000.

[5] G. Kipshidze, *et al.*, "Controlled growth of GaN nanowires by pulsed metalorganic chemical vapor deposition," *Applied Physics Letters*, vol. 86, pp. 033104-3, 2005.

[6] G. Cheng, *et al.*, "Current rectification in a single GaN nanowire with a well-defined p--n junction," *Applied Physics Letters*, vol. 83, pp. 1578-1580, 2003.

[7] S. D. Lester, *et al.*, "High dislocation densities in high efficiency GaN-based light-emitting diodes," *Applied Physics Letters*, vol. 66, pp. 1249-1251, 1995.

[8] R. Calarco, *et al.*, "Size-dependent Photoconductivity in MBE-Grown GaN−Nanowires," *Nano Letters*, vol. 5, pp. 981-984, 2005.

[9] O. Hayden, *et al.*, "Core–Shell Nanowire Light-Emitting Diodes," *Advanced Materials*, vol. 17, pp. 701-704, 2005.

[10] F. Qian, *et al.*, "Core/Multishell Nanowire Heterostructures as Multicolor, High-Efficiency Light-Emitting Diodes," *Nano Letters*, vol. 5, pp. 2287-2291, 2005.

[11] C. Mazuir and W. V. Schoenfeld, "Modeling of nitride based core/multishell nanowire light emitting diodes," *Journal of Nanophotonics*, vol. 1, pp. 013503-12, 2007.

[12] C. Mazuir and W. V. Schoenfeld, "Modeling standard techniques to improve core/multishell nanowire light emitting diodes efficiencies," San Diego, CA, USA, 2008, pp. 70560X-9.

[13] S. Nakamura, "GaN Growth Using GaN Buffer Layer," *Japanese Journal of Applied Physics*, vol. 30, p. L1705.

[14] S. Nakamura, *et al.*, "Si- and Ge-Doped GaN Films Grown with GaN Buffer Layers," *Japanese Journal of Applied Physics*, vol. 31, p. 2883.

[15] H. Amano, *et al.*, "Metalorganic vapor phase epitaxial growth of a high quality GaN film using an AlN buffer layer," *Applied Physics Letters*, vol. 48, pp. 353-355, 1986.

[16] G. Y. Zhang, *et al.*, "Relationship of background carrier concentration and defects in GaN grown by metalorganic vapor phase epitaxy," *Applied Physics Letters*, vol. 71, pp. 3376-3378, 1997.

[17] S. J. Pearton, *et al.*, "GaN: Processing, defects, and devices," *Journal of Applied Physics*, vol. 86, pp. 1-78, 1999.

[18] J. Oila, *et al.*, "Ga vacancies as dominant intrinsic acceptors in GaN grown by hydride vapor phase epitaxy," *Applied Physics Letters*, vol. 82, pp. 3433-3435, 2003.

[19] T. Hashizume and R. Nakasaki, "Discrete surface state related to nitrogen-vacancy defect on plasma-treated GaN surfaces," *Applied Physics Letters,* vol. 80, pp. 4564-4566, 2002.
[20] D. J. Carter and C. Stampfl, "Atomic and electronic structure of single and multiple vacancies in GaN nanowires from first-principles," *Physical Review B,* vol. 79, p. 195302, 2009.
[21] S. Nakamura, *et al.*, "Hole Compensation Mechanism of P-Type GaN Films," *Japanese Journal of Applied Physics,* vol. 31, p. 1258.
[22] H. Amano, *et al.*, "P-Type Conduction in Mg-Doped GaN Treated with Low-Energy Electron Beam Irradiation (LEEBI)," *Japanese Journal of Applied Physics,* vol. 28, p. L2112.
[23] S. Nakamura, *et al.*, "Thermal Annealing Effects on P-Type Mg-Doped GaN Films," *Japanese Journal of Applied Physics,* vol. 31, p. L139.
[24] P. Hacke, *et al.*, "Deep levels in the upper band-gap region of lightly Mg-doped GaN," *Applied Physics Letters,* vol. 68, pp. 1362-1364, 1996.
[25] U. Kaufmann, *et al.*, "Hole conductivity and compensation in epitaxial GaN:Mg layers," *Physical Review B,* vol. 62, p. 10867, 2000.
[26] P. Kozodoy, *et al.*, "Heavy doping effects in Mg-doped GaN," *Journal of Applied Physics,* vol. 87, pp. 1832-1835, 2000.
[27] L. B. Rowland, *et al.*, "Silicon doping of GaN using disilane," *Applied Physics Letters,* vol. 66, pp. 1495-1497, 1995.
[28] S. Dhara, *et al.*, "Blueshift of yellow luminescence band in self-ion-implanted n-GaN nanowire," *Applied Physics Letters,* vol. 84, pp. 3486-3488, 2004.
[29] E. F. Schubert, *et al.*, "Optical properties of Si-doped GaN," *Applied Physics Letters,* vol. 71, pp. 921-923, 1997.
[30] J. C. Zolper, *et al.*, "Electrical and structural analysis of high-dose Si implantation in GaN," *Applied Physics Letters,* vol. 70, pp. 2729-2731, 1997.
[31] W. Gotz, *et al.*, "Activation energies of Si donors in GaN," *Applied Physics Letters,* vol. 68, pp. 3144-3146, 1996.
[32] L. T. Romano, *et al.*, "Effect of Si doping on strain, cracking, and microstructure in GaN thin films grown by metalorganic chemical vapor deposition," *Journal of Applied Physics,* vol. 87, pp. 7745-7752, 2000.
[33] H. M. Ng, *et al.*, "The role of dislocation scattering in n-type GaN films," *Applied Physics Letters,* vol. 73, pp. 821-823, 1998.
[34] E. P. Pokatilov, *et al.*, "Confined electron-confined phonon scattering rates in wurtzite AlN/GaN/AlN heterostructures," *Journal of Applied Physics,* vol. 95, pp. 5626-5632, 2004.
[35] D. Camacho Mojica and Y.-M. Niquet, "Stark effect in GaN/AlN nanowire heterostructures: Influence of strain relaxation and surface states," *Physical Review B,* vol. 81, p. 195313, 2010.
[36] W. Han, *et al.*, "Synthesis of Gallium Nitride Nanorods Through a Carbon Nanotube-Confined Reaction," *Science,* vol. 277, pp. 1287-1289, 1997.
[37] C.-C. Chen, *et al.*, "Catalytic Growth and Characterization of Gallium Nitride Nanowires," *Journal of the American Chemical Society,* vol. 123, pp. 2791-2798, 2001.

[38] X. Duan and C. M. Lieber, "Laser-Assisted Catalytic Growth of Single Crystal GaN Nanowires," *Journal of the American Chemical Society,* vol. 122, pp. 188-189, 1999.
[39] M. S. Gudiksen, *et al.*, "Synthetic Control of the Diameter and Length of Single Crystal Semiconductor Nanowires," *The Journal of Physical Chemistry B,* vol. 105, pp. 4062-4064, 2001.
[40] X. L. Chen, *et al.*, "Radial growth dynamics of nanowires," *Journal of Crystal Growth,* vol. 222, pp. 586-590, 2001.
[41] H. Y. Peng, *et al.*, "Control of growth orientation of GaN nanowires," *Chemical Physics Letters,* vol. 359, pp. 241-245, 2002.
[42] J. C. Wang, *et al.*, "High-quality GaN nanowires synthesized using a CVD approach," *Applied Physics A: Materials Science & Processing,* vol. 75, pp. 691-693, 2002.
[43] Z. Zhong, *et al.*, "Synthesis of p-Type Gallium Nitride Nanowires for Electronic and Photonic Nanodevices," *Nano Letters,* vol. 3, pp. 343-346, 2003.
[44] Y. S. Park, *et al.*, "Electron trap level in a GaN nanorod p-n junction grown by molecular-beam epitaxy," *Applied Physics Letters,* vol. 88, pp. 192104-3, 2006.
[45] Y. S. Park, *et al.*, "Electrical transport properties of a nanorod GaN p-n homojunction grown by molecular-beam epitaxy," *Journal of Applied Physics,* vol. 103, pp. 066107-3, 2008.
[46] M. Boroditsky, *et al.*, "Surface recombination measurements on III--V candidate materials for nanostructure light-emitting diodes," *Journal of Applied Physics,* vol. 87, pp. 3497-3504, 2000.
[47] A. A. Talin and et al., "Transport characterization in nanowires using an electrical nanoprobe," *Semiconductor Science and Technology,* vol. 25, p. 024015, 2010.
[48] H. Moon-Ho and et al., "Contact characteristics in GaN nanowire devices," *Nanotechnology,* vol. 17, p. 2203, 2006.
[49] F. Qian, *et al.*, "Gallium Nitride-Based Nanowire Radial Heterostructures for Nanophotonics," *Nano Letters,* vol. 4, pp. 1975-1979, 2004.
[50] L. J. Lauhon, *et al.*, "Epitaxial core-shell and core-multishell nanowire heterostructures," *Nature,* vol. 420, pp. 57-61, 2002.
[51] X. Guo and E. F. Schubert, "Current crowding and optical saturation effects in GaInN/GaN light-emitting diodes grown on insulating substrates," *Applied Physics Letters,* vol. 78, pp. 3337-3339, 2001.
[52] H. Kim, *et al.*, "Lateral current transport path, a model for GaN-based light-emitting diodes: Applications to practical device designs," *Applied Physics Letters,* vol. 81, pp. 1326-1328, 2002.
[53] W. B. Joyce and S. H. Wemple, "Steady-State Junction-Current Distributions in Thin Resistive Films on Semiconductor Junctions (Solutions of [down triangle, open][sup 2][sub v] = [plus-minus]e[sup v])," *Journal of Applied Physics,* vol. 41, pp. 3818-3830, 1970.
[54] N. H. Fletcher, "Some Aspects of the Design of Power Transistors," *Proceedings of the IRE,* vol. 43, pp. 551-559, 1955.
[55] M. Auf der Maur, *et al.*, "TiberCAD: A new multiscale simulator for electronic and optoelectronic devices," *Superlattices and Microstructures,* vol. 41, pp. 381-385.

[56] V. Krishnamurthy and et al., "Robust and optimum designs of non-linearly tapered slow light couplers," *Journal of Optics A: Pure and Applied Optics,* vol. 11, p. 045102, 2009.
[57] J. F. Muth, *et al.*, "Absorption coefficient, energy gap, exciton binding energy, and recombination lifetime of GaN obtained from transmission measurements," *Applied Physics Letters,* vol. 71, pp. 2572-2574, 1997.
[58] I.-H. Lee, *et al.*, "Band-gap narrowing and potential fluctuation in Si-doped GaN," *Applied Physics Letters,* vol. 74, pp. 102-104, 1999.
[59] H. Nagai, *et al.*, "Hole trap levels in Mg-doped GaN grown by metalorganic vapor phase epitaxy," *Applied Physics Letters,* vol. 73, pp. 2024-2026, 1998.